Ecological Informatics 29 (2015) 77–91

Contents lists available at ScienceDirect

Ecological Informatics

journal homepage: www.elsevier.com/locate/ecolinf

Integrating hierarchical Bayes with phosphorus loading modelling

Yuko Shimoda, George B. Arhonditsis *

Ecological Modelling Laboratory, Department of Physical & Environmental Sciences, University of Toronto, Toronto, Ontario M1C 1A4, Canada

ARTICLE INFO

Article history:
Received 17 May 2015
Received in revised form 19 July 2015
Accepted 22 July 2015
Available online 30 July 2015

Keywords:
Total phosphorus
Bayesian hierarchical modelling
Phosphorus loading
Seasonal variability
Lake management

ABSTRACT

The causal linkage between lake productivity and phosphorus loading has provided the basis for a family of models that predict lake total phosphorus concentrations as a function of lake morphometric/hydraulic characteristics, such as the areal phosphorus loading rate, mean lake depth, fractional phosphorus retention and areal hydraulic loading. Most of these empirical models have been derived from "cross-sectional" datasets, comprising multiple point measurements or single averages from a number of lakes, and are typically used to predict changes within a single system at different points in time. This practice implicitly postulates that the large scale (cross-sectional) patterns described in the model are also representative of the dynamics of individual systems. In this study, we relax this assumption using a Bayesian hierarchical strategy that aims to accommodate the role of significant sources of variability (morphology, hydraulic regime). We first examine several hierarchical structures representing different characterizations of model error, parameter covariance, and prior distribution followed by the hyperparameters. Our analysis primarily highlights the robustness of the posterior group-level patterns to the hierarchical formulation developed. We also show that the delineation of homogeneous subsets of lakes with respect to their morphological/hydraulic characteristics and the subsequent integration with hierarchical frameworks may give empirical phosphorus retention/loading models with better predictive ability. We then present a complementary exercise that aims to accommodate the spatial and seasonal total phosphorus variability within individual systems, using a spatially-explicit simple mass-balance model forced with idealized sinusoidal loading. Our study concludes by advocating that the hierarchical Bayes provides a conceptually appealing framework to gradually accommodate different sources of variability and more prudently increase the complexity of simple empirical models.

1. Introduction

Vollenweider's (1975) eutrophication modelling work has spawned a family of predictive tools that link total phosphorus concentrations with lake morphometric/hydraulic characteristics (areal phosphorus loading rate, fractional phosphorus retention, mean lake depth, and areal hydraulic loading) and is often considered as one of the most influential contributions to the field of limnology. Despite their conceptual and structural simplicity, these empirical models represent important tools for the management of impaired lakes and the protection of unaffected waterbodies (Brett and Benjamin, 2008; Dillon and Molot, 1996; Reckhow and Chapra, 1983). The use of "cross-sectional" datasets, consisting of multiple point measurements or single averages from a number of lakes, is one of their appealing features as the significant intersystem variability typically leads to well-identified parameters and a fairly broad application domain (Prairie and Marshall, 1995). Another major characteristic of their integration with the lake management is their use for predicting within-system dynamics under the assumption that large-scale (among-system) variability, reflected by their parameter estimates, is also representative of the patterns characterizing individual systems (Cheng et al., 2010; Reckhow, 1993). The latter practice essentially postulates that the regulation of lake productivity by phosphorus inputs is the same among and within systems and therefore all the lakes in the dataset have identical behaviour.

The credibility of the inference drawn by "global-scale" models to address water quality issues in individual lakes has often been challenged, given that the variability within a single system is generally much smaller than across multiple systems and may be confounded by the seasonal patterns. In addition, the vast majority of the existing empirical models fail to accommodate the interplay between offshore and inshore sites in larger lakes. Nearshore areas represent transitional zones in that they can receive polluted inland waters from watersheds with significant agricultural, urban and/or industrial activities, while mixing with offshore waters having different biological and chemical characteristics (Shimoda et al., 2011). In the same context, the arrival of dreissenid mussels in many parts of the Laurentian Great Lakes has induced a major restructuring of the biophysical littoral environment with profound shifts on the retention and recycling of nutrients, thereby casting doubt on the suitability of simple mass-balance phosphorus models to serve as management tools (Hecky et al., 2004; Kim et al.,

* Corresponding author. Tel.: +1 416 208 4858; fax: +1 416 287 7279.
E-mail address: georgea@utsc.utoronto.ca (G.B. Arhonditsis).

http://dx.doi.org/10.1016/j.ecoinf.2015.07.005
1574-9541/

2013). Namely, because of their founding assumption that the lakes resemble to well-mixed reactors, it has been argued that the lack of distinction between nearshore and offshore regions and the adoption of lake-wide sedimentation rates fail to accurately reproduce the capacity of the "nearshore shunt" in modulating the particle and nutrient removal from the water column in space and time (Hecky et al., 2004).

Recognizing the structural inadequacies of the classical phosphorus loading models, the development of statistical techniques that relax the assumption of globally-common parameter estimation has been one of the priorities of the relevant modelling efforts. A characteristic example is the random coefficient linear regression model that uses random draws from a common probability distribution to obtain system-specific characterization (Judge et al., 1985; Swamy, 1971), thereby accommodating the behaviour of individual lakes and effectively reducing the prediction error compared to classical (global) models (Reckhow, 1993). More recently, Malve and Qian (2006) developed a Bayesian hierarchical linear model to assess the likelihood of compliance of Finnish lakes with chlorophyll *a* concentration standards under different nitrogen and phosphorus loading conditions. This modelling strategy offered the ability to transfer information across systems and support predictions in lakes with few observations and limited observational range, while the use of Bayesian inference allowed impartially assessing the uncertainty associated with parameter estimates and model predictions (Malve and Qian, 2006). Along the same line of reasoning, Cheng et al. (2010) introduced a Bayesian hierarchical configuration to evaluate the relative performance of seven lake phosphorus models, while achieving an optimal balance between site-specific (where limited local data is a problem) and globally-common (where heterogeneous systems in wide geographical areas are assumed to be identical) parameter estimates. The hierarchical framework led to significant improvement in the performance of the phosphorus retention/loading models against a cross-system dataset of 305 lakes, although the predictive statements derived for individual lakes still had a large error (Cheng et al., 2010).

In this study, our thesis is that the Bayesian hierarchical proposition offers a convenient means for addressing a variety of aquatic science and nutrient modelling problems in which partial, but not complete, commonality can be assumed among the modelled units. First, we examine several hierarchical formulations representing different characterizations of model error, parameter covariance, and prior distribution followed by the hyperparameters. This part of our analysis primarily aims to shed light on (i) the robustness of the posterior parameter patterns to the assumptions of the hierarchical formulation used; and (ii) the potential of the delineation of homogeneous subsets of lakes in regard to their morphological/hydraulic characteristics to provide empirical hierarchical models with better predictive ability. Second, we present a complementary exercise intended to accommodate the spatial and seasonal total phosphorus variability within individual systems, using a spatially-explicit simple mass-balance model forced with idealized sinusoidal loading. Striving for an improvement of the credibility of model-based eutrophication management, our study argues in favour of simple models that remain within the bounds of empirical parameter estimation and therefore can accommodate complete error analysis. The Bayesian hierarchical approach offers a flexible ad-hoc strategy to gradually increase model complexity and augment their explanatory value, whenever possible and relevant.

2. Methods

2.1. Cross-system TP (or "Vollenweider-type") model

The first part of our analysis builds upon the dataset compiled by Brett and Benjamin (2008) along with the key findings from the Bayesian hierarchical reanalysis presented by Cheng et al. (2010). The dataset consists of 305 North American and European lakes, collected from eight published, large-scale phosphorus mass-balance budgets. For each lake included in the dataset, we have an in-lake *TP* concentration, TP_{lake} ($\mu g\ L^{-1}$), the associated inflow weighted *TP* concentration, TP_{in} ($\mu g\ L^{-1}$), and the basic morphometric/hydrologic characteristics (i.e., lake volume, lake surface area, mean lake depth, inflow rate, hydraulic retention time). The configuration of our Bayesian hierarchical framework is based on the delineation of the homogeneous groups derived by Cheng et al.'s (2010) classification and regression tree (*CART*) analysis, which identified the important morphometric (volume, mean depth, surface area) and hydrologic (hydraulic retention time, inflow rates) characteristics along with the ideal cutoff levels of the ambient *TP* variability. In particular, we present our hierarchical modelling exercise under two grouping schemes. The first one simply discriminates between deep and shallow lakes based on Cheng et al.'s (2010) first splitting condition at a critical mean lake depth of 10.3 m, while the second classification comprises the eight terminal nodes of the same *CART* analysis (see lake characteristics in Table 1 of the Electronic Supplementary Material). Among the different formulations proposed in the limnological literature (Brett and Benjamin, 2008; Cheng et al., 2010), we used the TP_{lake} model that postulates the phosphorus loss term, σ, to be represented by an expression of the form $\sigma = k \cdot {\tau_w}^{x-1}$, where τ_w is the mean hydraulic retention time (yr) and k, x are adjustable parameters (see Appendix A). Several phosphorus modelling studies over the past four decades have rendered support to this model (Chapra and Reckhow, 1979; Larsen and Mercier, 1976; Uttormark and Hutchins, 1978; Vollenweider, 1976; Walker, 1977), which was also found to be the most parsimonious construct with the present dataset (Brett and Benjamin, 2008; Cheng et al., 2010).

In our dataset, there are $i = 1, 2, \cdots, N$ separate lakes, with $N = 305$, each classified in one of the m lake types or groups (2 or 8) delineated by the *CART* analysis. In our predictive model, different lakes within the same lake type are viewed as lakes with identical behaviour and therefore share the same model parameters. Because our dataset contains single *TP* observations for each system, presumably representative of its typical phosphorus loading and hydrological conditions, our assumption postulates that a particular model structure and parameter specification is sufficient to accommodate the observed variability within each lake group. On the other hand, the same assumption does not hold true for lakes that have been classified in different lake groups, although some similarity is not ruled out. Therefore, estimates of group-specific model parameters are expressed in terms of a common prior distribution. In other words, we assume that lake type-specific model parameters are random variables from a common distribution. Computationally, it is natural to model the data hierarchically. That is, *TP* average values of individual lakes are modelled conditional on lake group-specific model parameter values, the lake group-specific model parameter values are modelled conditional on one parameter distribution reflecting all lakes in our dataset, which are themselves modelled conditional on hyperparameters that represent the hypothetical lake population from which the lakes in our dataset have been sampled. An important feature of the hierarchical model is that the hierarchical probability distribution imposes dependence among parameters, which allows a hierarchical model to have enough parameters to form a realistic model without overfitting the data (Borsuk et al., 2001). The inference drawn and the robustness of the parameter estimates of the cross-system *TP* model was evaluated under five hierarchical formulations summarized as follows:

(i) Classical hierarchical model:

$$\log\left(y_{ij}\right) \sim N\left(f\left(\theta_j, x_{ij}\right), \tau^2\right)$$
$$\theta_j \sim N\left(\theta, {\sigma_j}^2\right)$$
$$\theta_j \sim N\left(\mu, \sigma^2\right)$$
$$\mu \sim N(0, 10000) \quad \sigma^2 \sim IG(0.001, 0.001)$$
$${\sigma_j}^2 \sim IG(0.001, 0.001)$$
$$\tau^2 \sim IG(0.001, 0.001)$$
$$i = 1, \ldots, 305 \quad j = 1, 2 (\text{or } 8)$$

Table 1
Root mean square error (*RMSE*) and Nash Sutcliffe Model Efficiency (*NSME*) values of phosphorus loading models with lake classifications in two and eight groups. Numbers in parentheses represent the *RMSE* values (μg *TP* L^{-1}) when the lake *TP* concentrations in the corresponding groups were predicted with the two-group classification. The morphological/hydraulic and water quality characteristics of the eight lake types are provided in the Electronic Supplementary Material.

	Model 1 — Classical	Model 2 — Informative Global Prior	Model 3 — Alternative Model Error	Model 4 — Multivariate Normal	Model 5 — Multivariate Normal & Alternative Error
Two-group lake classification					
RMSE (overall)	185.2	185.9	191.2	186.6	191.9
NSME (overall)	−0.113	−0.120	−0.187	−0.130	−0.195
RMSE ($\bar{z} \le 10.3$ m)	229.0	228.2	234.8	229.1	235.7
NSME ($\bar{z} \le 10.3$ m)	−0.231	−0.223	−0.295	−0.233	−0.305
RMSE ($\bar{z} > 10.3$ m)	37.87	37.84	37.49	37.86	37.49
NSME ($\bar{z} > 10.3$ m)	0.613	0.613	0.620	0.613	0.620
Eight-group lake classification					
RMSE (overall)	173.1	172.3	172.3	175.5	179
NSME (overall)	0.015	0.024	0.024	−0.009	−0.050
RMSE Group I	519.9 (567.7)	517.3	517.3	529.1	540.4
NSME Group I	−1.155	−1.133	−1.133	−1.232	-1.329
RMSE Group II	45.81 (49.20)	45.75	45.75	45.78	47.83
NSME Group II	0.311	0.313	0.313	0.312	0.249
RMSE Group III	45.69 (51.70)	45.70	45.70	45.81	48.22
NSME Group III	0.683	0.682	0.682	0.681	0.647
RMSE Group IV	96.03 (100.5)	96.08	96.08	97.09	96.28
NSME Group IV	0.788	0.788	0.788	0.783	0.787
RMSE Group V	28.44 (28.51)	28.51	28.51	28.65	28.77
NSME Group V	0.650	0.648	0.648	0.645	0.642
RMSE Group VI	38.96 (38.92)	38.95	38.95	38.90	38.57
NSME Group VI	0.612	0.612	0.612	0.613	0.620
RMSE Group VII	47.05 (57.19)	47.07	47.07	47.58	47.57
NSME Group VII	0.578	0.577	0.577	0.568	0.568
RMSE Group VIII	7.421 (9.254)	7.406	7.406	7.555	8.122
NSME Group VIII	0.355	0.358	0.358	0.332	0.228

where $log(y_{ij})$ is the observed log-transformed TP_{lake} value from the lake i in the group (lake type) j; $f(\theta_j, x_{ij})$ is the empirical phosphorus loading model used; τ^2 is the model error variance; θ_j is the group-specific parameter set; x_{ij} represents the vector of lake-specific input variables, i.e., the inflow weighted *TP* concentration, TP_{in} (μg L^{-1}), and the mean hydraulic retention time, τ_w (yr); θ corresponds to the global parameters; σ_j^2 is the group-specific variance or alternatively the among-lake variance of model parameters for the lake type j; μ and σ^2 are the mean and variance of the global parameter distributions (or the hyperparameters), respectively; $N(0, 10000)$ is the normal distribution with mean 0 and variance 10000, and $IG(0.001, 0.001)$ is the inverse gamma distribution with shape and scale parameters of 0.001. The prior distributions for τ^2, σ^2, and μ are considered "non-informative" or vague. The latter treatment of the hyperparameters differs from the approach followed by Cheng et al. (2010), in which both μ and σ^2 are treated as known inputs and were associated (in varying degrees) with the corresponding least square estimates reported by Brett and Benjamin (2008; see their Table 5). A second major difference is that Cheng et al. (2010) treated the group-specific parameters θ_j as draws from normal distributions with unknown means and known variances set equal to a very high value (=10,000), whereas both first and second order moments with the current hierarchical configuration represent stochastic nodes that are subject to updating.

(ii) Hierarchical model with informative global prior:

$$\log\left(y_{ij}\right) \sim N\left(f\left(\theta_j, x_{ij}\right), \tau^2\right)$$
$$\theta_j \sim N\left(\theta, {\sigma_j}^2\right)$$
$$\theta \sim N\left(\mu, \sigma^2\right)$$
$$\mu \sim N\left(\mu_{LS}, {\sigma_{LS}}^2\right) \sigma^2 \sim IG(0.001, 0.001)$$
$$\sigma_j{}^2 \sim IG(0.001, 0.001)$$
$$\tau^2 \sim IG(0.001, 0.001)$$
$$i = 1, \ldots, 305 \quad j = 1, 2(\text{or } 8).$$

The difference between the second hierarchical structure and the classical one is the use of an informative prior for the hyperparameter μ. In particular, the specification of the vectors $\mu_{LS} = [\mu_k, \mu_x]$ and $\sigma^2_{LS} = [\sigma_k^2, \sigma_x^2]$ was based on the assumption that 68% of the corresponding values are lying within the least square mean ± standard error ranges reported by Brett and Benjamin (2008). Strictly speaking, this assumption implies that information from the same dataset is used twice (formulation of prior hyperparameter distributions, model updating), and thus the second hierarchical formulation is purposely designed to offer a reference strategy for comparing the robustness of posterior parameter patterns. It is also worth noting that relative to the Cheng et al.'s (2010) parameterization, the present hierarchical model allocates all the background information to the global means, while the corresponding variances were assigned "non-informative" inverse gamma priors.

(iii) Hierarchical model with alternative model structural error:

$$\log\left(y_{ij}\right) \sim N\left(f\left(\theta_j, x_{ij}\right), {\tau_{ij}}^2\right)$$
$$\theta_j \sim N\left(\theta, {\sigma_j}^2\right)$$
$$\theta \sim N\left(\mu, \sigma^2\right)$$
$$\mu \sim N(0, 10000) \sigma^2 \sim IG(0.001, 0.001)$$
$$\sigma_j{}^2 \sim IG(0.001, 0.001)$$
$$\log\left({\tau_{ij}}^{-2}\right) = \varphi_0 + \varphi_1\left(1/TP_{inij}\right)$$
$$\varphi_0, \varphi_1 \sim N(0, 10000)$$
$$i = 1, \ldots, 305 \quad j = 1, 2(\text{or } 8).$$

The third hierarchical structure is practically identical to the classical one with the only difference being the characterization of the structural error τ^2. In particular, we specify a regression model that expresses the logarithm of lake-specific error precision (1/variance) as a linear function of the inverse of the corresponding inflow weighted *TP* concentration. The slope, φ_1, and intercept, φ_0, of the latter model are assigned flat normal priors. This equation postulates a pattern of rectangular hyperbola

between the model standard error and the inflow weighted *TP* concentration.

(iv) Hierarchical model with multivariate normal parameter prior:

$$\log\left(y_{ij}\right) \sim N\left(f\left(\theta_j, x_{ij}\right), \tau^2\right)$$
$$\theta_j \sim MN(\theta, \Sigma_\theta)$$
$$\theta \sim MN(\mu, \Sigma_\mu)$$
$$\mu = [0, 0], \Sigma_\mu = \begin{bmatrix} 10000 & 0 \\ 0 & 10000 \end{bmatrix}$$
$$\Sigma_\theta \sim IW(R, 2) R = \begin{bmatrix} 0.1 & 0 \\ 0 & 0.1 \end{bmatrix}$$
$$\tau^2 \sim IG(0.001, 0.001)$$
$$i = 1, \ldots, 305 \quad j = 1, 2(\text{or } 8).$$

Relative to the classical hierarchical model, the fourth configuration explicitly accommodates the covariance between the model parameters k and x at the lake-type (group) level. The covariance matrix Σ_θ is assigned an inverse Wishart prior, in which the scale matrix R represents an assessment of the order of magnitude of the covariance matrix between the two group-specific parameters. To represent lack of confidence on the existing information, we chose two degrees of freedom for this distribution (n = 2), which is equal to the rank of the matrix. A second major difference is that the fourth hierarchical model does not explicitly consider the lake type-specific model parameter variance σ_j^2; that is, the among-lake variance of model parameters for each lake type j is now replaced by two stochastic nodes (diagonal elements of Σ_θ) that capture the variability of the model parameters k, x across the all the lake in our dataset. A multivariate normal distribution with known mean vector and covariance matrix is used as a global prior; the mean values were set equal to zero, while the diagonal elements of the covariance matrix were assigned high values (=10,000) and the non-diagonal entries were set equal to zero.

(v) Hierarchical model with multivariate normal parameter prior and alternative structural error:

$$\log\left(y_{ij}\right) \sim N\left(f\left(\theta_j, x_{ij}\right), {\tau_{ij}}^2\right)$$
$$\theta_j \sim MN(\theta, \Sigma_\theta)$$
$$\theta \sim MN(\mu, \Sigma_\mu)$$
$$\mu = [0, 0], \Sigma_\mu = \begin{bmatrix} 10000 & 0 \\ 0 & 10000 \end{bmatrix}$$
$$\Sigma_\theta \sim IW(R, 2) R = \begin{bmatrix} 0.1 & 0 \\ 0 & 0.1 \end{bmatrix}$$
$$\log\left({\tau_{ij}}^{-2}\right) = \varphi_0 + \varphi_1\left(1/TP_{inij}\right)$$
$$\varphi_0, \varphi_1 \sim N(0, 10000)$$
$$i = 1, \ldots, 305 \quad j = 1, 2(\text{or } 8).$$

The final hierarchical model combines the multivariate normal characterization of the two parameters k and x with the specification of the logarithm of the structural error precision as a linear function of the inverse of the inflow weighted *TP* concentration.

2.2. Continuously stirred tank reactor model forced with sinusoidal loading

The second part of our analysis is based on a spatially-explicit, mass-balance model forced with idealized sinusoidal loading to predict total phosphorus concentrations. The model was originally introduced by Gudimov et al. (2012) to represent the epilimnion of Lake Simcoe, Ontario, Canada, as a feedforward system of continuously stirred tank reactors (Fig. 2). [A brief description of the basic limnological characteristics of Lake Simcoe is provided in the Electronic Supplementary Material.] A central feature of the feedforward configuration is the postulation of a net unidirectional flow within the framework of serial reactors considered; an assumption that was critically examined by Gudimov et al. (2012). The analytical solution of the differential equations that describe the *TP* balance in the three segments (S_1, S_2, S_3) is determined by the exogenous loading sources and three sinks (outflow, reaction, and settling) that deplete the ambient phosphorus levels in the system is:

$$\text{For } j = S_1, S_2, S_3 \quad TP_{tij} = \frac{W_{avg(ij)}}{\lambda_{(ij)} V_{(ij)}} + \frac{W_{amplitude\,(ij)}}{V_{(ij)}\sqrt{{\lambda_{(ij)}}^2 + \omega^2}} \sin\left[\omega t - \theta_{(ij)} - \phi_{(ij)}(\omega)\right]$$

$$\phi_{(ij)}(\omega) = \arctan\left(\frac{\omega}{\lambda_{(ij)}}\right)$$

$$\lambda_{(ij)} = \kappa_{1(ij)} + \kappa_{2(ij)}\kappa_{1(ij)} = \frac{Q_{(ij)}}{V_{(ij)}}\kappa_{2(ij)} = k_{(ij)} + \frac{v_{(j)}}{H_{(j)}}$$

in which TP_{tij} is the total phosphorus concentration (μg L^{-1}) in segment j, year i, and day t; $W_{avg(ij)}$ is the mean loading (tonnes day^{-1}) entering the segment j in year i; $W_{amplitude(ij)}$ corresponds to the amplitude around the mean loading $W_{avg(ij)}$ (tonnes day^{-1}); $\lambda_{(ij)}$ is the total loss rate (day^{-1}); $V_{(ij)}$ is the volume (m^3) of segment j in year i; $\theta_{(ij)}$ represents the phase shift (radians) of the loading from the standard wave; $\varphi_{(ij)}(\omega)$ is an additional phase shift related to the segment-specific response; and ω denotes the angular frequency (radians day^{-1}) of the loading oscillation; $Q_{(ij)}$ is the volumetric outflow rate (m^3 day^{-1}) from segment j in year i; $\nu_{(j)}$ represents the settling velocity (m day^{-1}) in segment j; $H_{(j)}$ is the mean depth (m) of the segment j; and $k_{(ij)}$ denotes the first-order reaction coefficient (day^{-1}) in segment j and year i. In a similar manner, the analytical solutions for the *TP* concentrations in day t in the other two sections are as follows:

$$\begin{aligned}\text{For } k = S_4 \quad TP_{tik} = {} & \sum_j \frac{Q_{(ij)} W_{avg(ij)}}{\lambda_{(ij)} V_{(ij)} \lambda_{(ik)} V_{(ik)}} + \frac{W_{avg(ik)}}{\lambda_{(ik)} V_{(ik)}} \\ & + \frac{W_{amplitude\,(ik)}}{V_{(ik)}\sqrt{{\lambda_{(ik)}}^2 + \omega^2}} \sin\left[\omega t - \theta_{(ik)} - \phi_{(ik)}(\omega)\right] \\ & + \sum_j \frac{Q_{(ij)} W_{amplitude\,(ij)}}{V_{(ij)} V_{(ik)}\sqrt{{\lambda_{(ij)}}^2 + \omega^2}\sqrt{{\lambda_{(ik)}}^2 + \omega^2}} \\ & \times \sin\left[\omega t - \theta_{(ij)} - \phi_{(ij)}(\omega) - \phi_{(ik)}(\omega)\right]\end{aligned}$$

$$\begin{aligned}\text{For } l = S_5 \quad TP_{til} = {} & \sum_j \frac{Q_{(ik)} Q_{(ij)} W_{avg(ij)}}{\lambda_{(il)} V_{(il)} \lambda_{(ij)} V_{(ij)} \lambda_{(ik)} V_{(ik)}} + \frac{Q_{(ik)} W_{avg(ik)}}{\lambda_{(il)} V_{(il)} \lambda_{(ik)} V_{(ik)}} \\ & + \frac{W_{avg(il)}}{\lambda_{(il)} V_{(il)}} + \frac{W_{amplitude\,(il)}}{V_{(il)}\sqrt{{\lambda_{(il)}}^2 + \omega^2}} \sin\left[\omega t - \theta_{(il)} - \phi_{(il)}(\omega)\right] \\ & + \frac{Q_{(ik)} W_{amplitude\,(ik)}}{V_{(il)} V_{(ik)}\sqrt{{\lambda_{(ik)}}^2 + \omega^2}\sqrt{{\lambda_{(il)}}^2 + \omega^2}} \\ & \times \sin\left[\omega t - \theta_{(ik)} - \phi_{(ik)}(\omega) - \phi_{(il)}(\omega)\right] \\ & + \sum_j \frac{Q_{(ik)} Q_{(ij)} W_{amplitude\,(ij)}}{V_{(il)} V_{(ij)} V_{(ik)}\sqrt{{\lambda_{(ij)}}^2 + \omega^2}\sqrt{{\lambda_{(ik)}}^2 + \omega^2}\sqrt{{\lambda_{(il)}}^2 + \omega^2}} \\ & \times \sin\left[\omega t - \theta_{(ij)} - \phi_{(ij)}(\omega) - \phi_{(ik)}(\omega) - \phi_{(il)}(\omega)\right].\end{aligned}$$

The hierarchical formulation used to accommodate the spatio-temporal variability of the *TP* concentrations was specified as follows:

$$log(TP_{tij}) \sim N\left(f\left(\kappa_{1(ij)}, \kappa_{2(ij)}, W_{avg(ij)}, W_{amplitude(ij)}, \theta_{(ij)}\right), \tau^2\right)$$
$$\tau^2 \sim IG(0.001, 0.001)$$
$$\kappa_{1(ij)} \sim N\left(\kappa_{1j}, {\sigma_{\kappa 1j}}^2\right)$$
$$\kappa_{2(ij)} \sim N\left(\kappa_2, {\sigma_{\kappa 2j}}^2\right) \kappa_2 \sim N\left(\kappa_{2\mu}, {\sigma_{\kappa 2}}^2\right)$$
$$\kappa_{2\mu} \sim N(0, 10000), \sigma_{\kappa 2}^2 \sim G(0.001, 0.001), {\sigma_{\kappa 2j}}^2 \sim IG(0.001, 0.001)$$
$$W_{avg(ij)} \sim N\left(W_{avgML(ij)}, {\Sigma_{Tot(ij)}}^2\right)$$
$$\Sigma_{Tot(ij)}^2 = {\sigma_{W(ij)}}^2 + {\sigma_{Wavg(ij)}}^2$$
$$W_{amplitude(ij)} \sim N\left(W_{amplitudeML(ij)}, {\sigma_{amplitude(ij)}}^2\right)$$
$$\theta_{(ij)} \sim N\left(\theta_{ML(ij)}, {\sigma_{\theta(ij)}}^2\right)$$
$$i=1,\ldots,5 j=1,\ldots,5 t=1,\ldots,7$$

where TP_{tij} corresponds to the average *TP* concentration at segment *j*, year *i*, and day *t* (samples collected from April to October from 1999 to 2003); τ^2 denotes the structural error variance of the seasonally-forced *TP* model; $\kappa_{1(ij)}$ is the net outflow rate from segment *j* at year *i*; the κ_{1j} and $\sigma_{\kappa 1j}$ correspondingly denote the segment-specific average flushing rates and the associated interannual variability, as calculated from the respective water balance budgets; κ_{2ij} is the net *TP* loss rate in segment *j* at year *i*; κ_2 represents the hyperparameter or the lakewide *TP* loss rate; $\sigma^2_{\kappa 2j}$ is the segment-specific variance, accounting for the year-to-year variability of the sedimentation rates within each segment; and $\kappa_{2\mu}$ and $\sigma^2_{\kappa 2}$ are the mean and variance of the global parameter distribution, respectively. The normal prior distribution assigned to the parameter $\kappa_{2\mu}$ and the inverse gamma distributions assigned to the parameters $\sigma^2_{\kappa 2}$ and $\sigma^2_{\kappa 2j}$ were flat or uninformative. The mean (W_{avgij}), amplitude ($W_{amplitudeij}$), and phase shift (θ_{ij}) values of the phosphorus loading at segment *j*, year *i* and day *t* were drawn from normal distributions in which the mean values ($W_{avgMLij}$, $W_{amplitudeMLij}$, θ_{MLij}) and error variances ($\sigma_{Wavgij}{}^2$, $\sigma_{amplitudeij}{}^2$, $\sigma_{\theta ij}{}^2$) were the maximum likelihood estimators obtained from fitting sinusoidal functions to the corresponding monthly loading data. The normal distributions of the mean annual loading (W_{avgij}) also considered the estimates of model error variance ($\sigma_{Wij}{}^2$) obtained from the maximum likelihood fitting exercise. In brief, the statistical calibration framework of the feedforward model accommodates the spatial and year-to-year *TP* variability with segment- and year-specific estimates of the sedimentation rate and water residence time, while its mathematical structure postulates that the *TP* seasonal patterns are primarily regulated by the within-year variability of the inflowing phosphorus from the adjacent watershed.

2.3. Model computations

Sequences of realizations from the posterior distributions of all of the models examined were obtained using Markov chain Monte Carlo (*MCMC*) simulations (Gilks et al., 1998). Specifically, we used the general normal-proposal Metropolis algorithm as implemented in the WinBUGS software; this algorithm is based on a symmetric normal proposal distribution, whose standard deviation is adjusted over the first 4000 iterations such as the acceptance rate ranges between 20 and 40% (Lunn et al., 2000). We used three chain runs of 100,000 iterations and samples were taken after the *MCMC* simulation converged to the true posterior distribution. Convergence of the *MCMC* chains was checked using the Brooks–Gelman–Rubin (*BGR*) scale–reduction factor (Brooks and Gelman, 1998). The *BGR* factor is the ratio of between-chain variability to within chain variability. The chains have converged when the upper limits of the *BGR* factor are close to one. Generally, we noticed that the sequences converged very rapidly (≈1000 iterations), and the summary statistics reported in this study were based on the last 95,000 draws by keeping every 10th iteration (thin = 10) to avoid serial correlation. The accuracy of the posterior parameter values was inspected by assuring that the Monte Carlo error (an estimate of the difference between the mean of the sampled values and the true posterior mean; see Lunn et al., 2000) for all parameters was less than 5% of the sample standard deviation (Spiegelhalter et al., 2002).

3. Results-discussion

3.1. What additional insights do we gain from the hierarchical configuration of phosphorus loading models?

The model fit assessment for the Bayesian hierarchical formulations, founded upon the distinction between shallow (≤10.3) and deeper (>10.3) lakes, is presented in Table 1. Generally, the application of the phosphorus loading/retention model to the shallow lakes resulted in distinctly higher root mean square error (*RMSE*) (>228 μg *TP* L^{-1}) and negative Nash Sutcliffe Model Efficiency (*NSME*) (<−0.220) values relative to the deeper ones (*RMSE* ≈ 38 μg *TP* L^{-1} and *NSME* > 0.615). The classical hierarchical formulation, the one with the informative global prior, and the hierarchical configuration with multivariate normal parameter prior resulted in nearly identical model performance (*RMSE* ≈ 185 μg *TP* L^{-1}). By contrast, the two formulations with structural error expressed as a function of the inflow weighted *TP* concentration were characterized by somewhat inferior fit (*RMSE* > 190 μg *TP* L^{-1}), which is directly related to their distinctly weaker performance with the shallow lakes (*RMSE* ≈ 235 μg *TP* L^{-1}). The refinement of the lake classification into eight groups led to an improvement of the overall model performance (Table 1, Fig. 1). In particular, the comparison between observed and predicted log-transformed *TP* concentrations indicated that the highest r^2 value was obtained with Group III, 0.900, and the lowest one with Group VIII, 0.529 (Fig. 1). On the other hand, the lowest error (*RMSE* ≈ 7.5 μg *TP* L^{-1}) was found with the group of lakes deeper than 10.3 m and hydraulic retention time longer than 17.8 years (Group VIII), followed by the group of lakes with mean depth between 1.65 m and 10.3 m and surface area greater than 20.3 km^2 or Group V (*RMSE* ≈ 28.5 μg *TP* L^{-1}). Nonetheless, the former group was characterized by distinctly lower *NSME* values (0.228–0.358) relative to the latter one (>0.640). The shallow lakes with mean depth lower than 1.65 m (Group I) were again characterized by the highest *RMSE* values 517–540 μg *TP* L^{-1}. Notably, the same group resulted in negative *NSME* values, which suggests that the average value of the corresponding data subset allows drawing better predictions than the model itself! High discrepancy between measured and modelled *TP* concentrations was also found with the group of lakes with surface area between 0.68 km^2 and 20.3 km^2, and hydraulic retention time longer than 0.17 years or Group IV (*RMSE* ≈ 96 μg *TP* L^{-1}). The model error with the rest of the lake types ranged from 38–48 μg *TP* L^{-1}. Similar to the previous classification scheme with two nodes, the classical hierarchical formulation with flat or informative global priors outperformed the models with the alternative structural error characterization. Based on the classical hierarchical model, we also examined which of the eight groups demonstrated the greatest improvement after refining our analysis from the second- to the eight-lake categorization scheme (numbers in parentheses in Table 1). The shallow lakes with depth lower than 1.65 m (Group I) displayed a substantial reduction of the corresponding *RMSE* value (568 versus 519 μg *TP* L^{-1}), relative to the *TP* predictions derived when they are pooled within a more heterogeneous assemblage of lakes. Distinct improvements were also found with the Group VII (57.2 versus 47.05 μg *TP* L^{-1}) and Group III (51.7 versus 45.4 μg *TP* L^{-1}), whereas the rest of the groups were characterized by fairly similar performance between the two parameterizations.

Generally, the two-group hierarchical configuration of the phosphorus loading model resulted in group-specific posterior mean parameter estimates that were relatively similar to the corresponding global parameter values, i.e., k_1 = 1.07 $year^{-0.52}$–1.13 $year^{-0.50}$ and x_1 = 0.50–0.52 for the shallow lakes, k_2 = 1.08 $year^{-0.47}$–1.14 $year^{-0.46}$ and x_2 = 0.46–0.47 for the deeper ones (Table 2). We also highlight the high identification levels of the $k_{1(2)}$ and $x_{1(2)}$ means, as depicted by their fairly low coefficient of variation values of 10–11% and 10–13%, respectively. By contrast, the posterior estimates of the group-specific standard deviations of the two parameters, σ_{kj} and σ_{xj} with *j* = 1,2, were poorly identified and the same was true for the rest of the stochastic nodes included in the two group hierarchical formulations. On a final note, the posterior estimates for the parameters φ_0 (= 1.22 ± 0.10) and φ_1 (= 3.65 ± 2.37) suggest that the lake-specific model structural error ($\tau_{ij}{}^2$) is approximately equal to 0.38 (*TP* concentrations in logarithmic units) when the phosphorus loading lies in very low levels (<5 μg *TP* L^{-1}), whereas a plateau within the range of 0.52–0.55 log_e(μg *TP* L^{-1}) is reached when the inflow weighted *TP* concentrations exceed a threshold of 40 μg *TP* L^{-1}.

Notwithstanding the substantial complexity increase of the hierarchical formulations, the consideration of eight homogeneous groups led to a significant improvement of the identification patterns of the

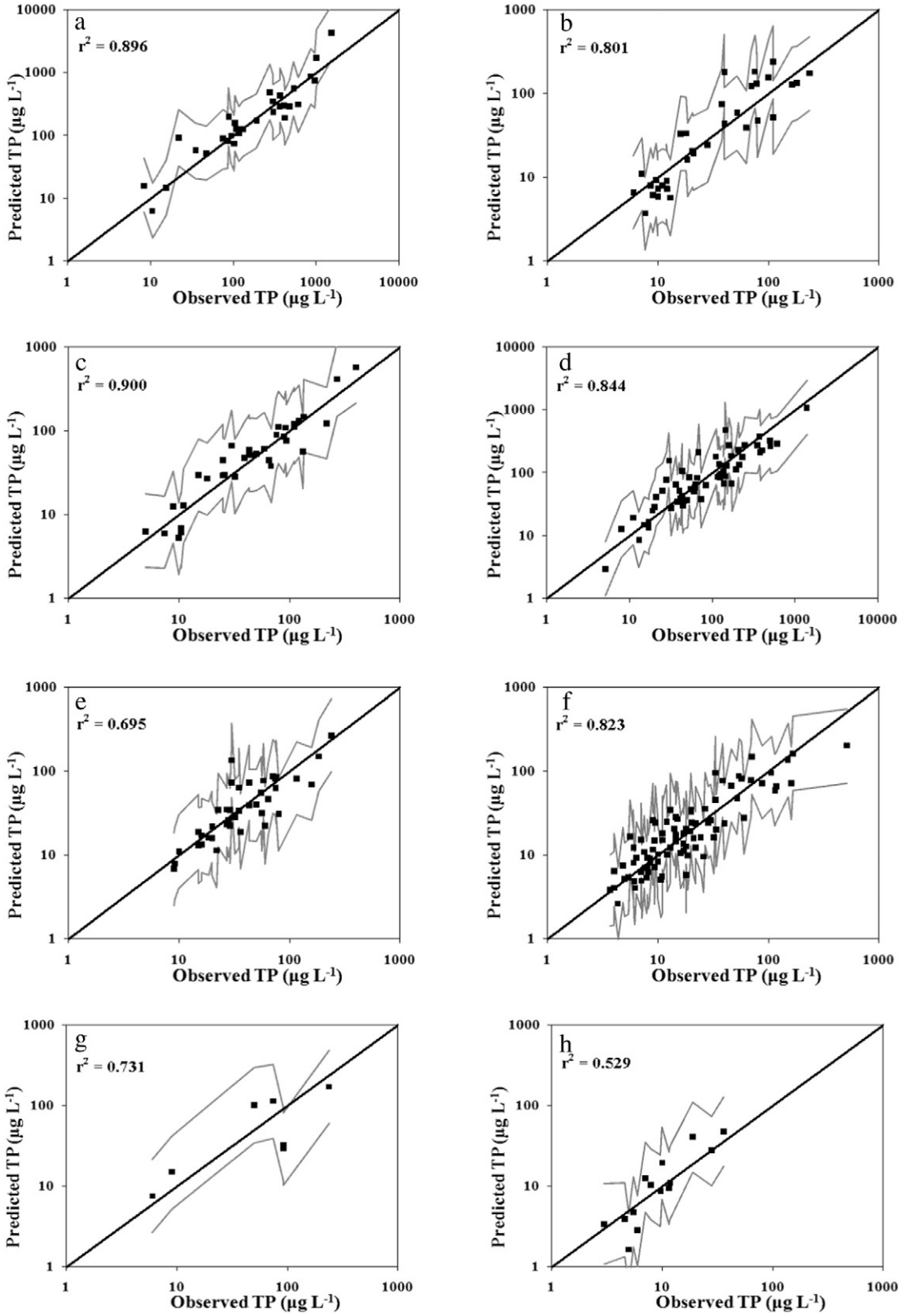

Fig. 1. Observed versus median predicted lake total phosphorus (TP_{lake}) concentrations [µg L^{-1}] for the eight groups delineated from the Cheng et al. (2010) CART analysis. Grey lines correspond to the 2.5 and 97.5% credible intervals. The diagonal line represents the perfect fit between predicted medians and observed values. The eight groups represent lakes with: (*a*) mean depth lower than 1.65 m; (*b*) mean depth between 1.65 m and 10.3 m and surface area lower than 1.47 km^2; (*c*) mean depth between 1.65 m and 10.3 m, surface area between 1.47 km^2 and 20.3 km^2, and hydraulic retention time shorter 0.17 years; (*d*) mean depth between 1.65 m and 10.3 m, surface area between 0.68 km^2 and 20.3 km^2, and hydraulic retention time longer than 0.17 years; (*e*) mean depth between 1.65 m and 10.3 m and surface area greater than 20.3 km^2; (*f*) mean depth greater than 10.3 m and hydraulic retention time shorter than 9.8 years; (*g*) mean depth greater than 10.3 m and hydraulic retention time between 9.8 years and 17.8 years; (*h*) mean depth greater than 10.3 m and hydraulic retention time longer than 17.8 years.

Table 2
Lake phosphorus loading model: summary statistics of the posterior parameter distributions for the five hierarchical model configurations founded upon the distinction between shallow ($\bar{z} \leq 10.3$ m) and deep lakes ($\bar{z} \geq 10.3$ m).

	Model 1 — Classical		Model 2 — Informative global Prior		Model 3 — Alternative model Error		Model 4 — Multivariate Normal		Model 5 — Multivariate Normal & Alternative Error	
	Mean	SD	Mean	SD	Mean	SD	Mean	SD	Mean	SD
k_1	1.13	0.09	1.13	0.09	1.07	0.10	1.13	0.10	1.07	0.10
k_2	1.13	0.12	1.13	0.11	1.08	0.12	1.14	0.12	1.08	0.12
x_1	0.50	0.07	0.50	0.06	0.52	0.07	0.51	0.07	0.52	0.07
x_2	0.46	0.05	0.46	0.04	0.47	0.05	0.46	0.05	0.47	0.05
k	1.22	1.08	1.12	0.13	1.20	2.05	1.15	0.34	1.09	0.33
x	0.57	0.89	0.48	0.95	0.57	0.64	0.52	0.32	0.54	0.41
σ_{k1}	1.45	20.26	2.6	123.1	1.40	20.92				
σ_{k2}	1.65	25.46	1.1	26.4	1.97	36.61				
σ_{x1}	7.19	498.6	0.55	4.74	1.05	11.31				
σ_{x2}	1.10	11.98	0.70	9.11	1.14	16.32				
σ_k	723	43420	0.79	8.84	59.84	548.40	0.37	0.35	0.38	0.40
σ_x	190	10290	1.00	36.84	84.64	1170	0.36	0.38	0.37	0.51
σ_{kx}							0.01	0.64	0.03	0.94
μ_k	11.4	26.5	1.12	0.07	11.61	27.26				
μ_x	11.3	27.3	0.47	0.04	11.16	26.45				
σ	0.52	0.02	0.52	0.02			0.52	0.02		
φ_1					3.65	2.38			3.64	2.37
φ_0					1.22	0.10			1.22	0.10

stochastic nodes examined. Drawing parallels with Gelman and Hill (2007; pages 476–480), we calculated the degree to which the *j* group-specific parameter estimates are pooled together (based on the global mean) rather than estimated separately (based on the raw data of each lake type). Counter to Gelman and Hill's (2007) Eq. (21.13) though, the pooling factors of the first three hierarchical formulations are calculated by normalizing the standard error (*se*) of the deviance of the lake group-specific parameter estimates from the global mean by the corresponding parameter variance σ_j^2, $\lambda_{\theta j} = \frac{(se(\theta_j - \theta))^2}{\sigma_j^2}$. The values of these pooling factors are not directly comparable with those derived by the multivariate normal parameter specification, which are based on the typical standardization over the diagonal entries of the covariance matrix Σ_θ, $\lambda_{\theta j} = \frac{(se(\theta_j - \theta))^2}{\sigma_\theta^2}$. Plotting the latter pooling factors against the sample size of the eight lake types considered (Fig. S1), we can infer that the Group VII with small sample size ($n = 7$) has high pooling factors (that is, the parameter estimates are halfway or closer to the global mean) followed by Group III ($n = 35$) and Group I ($n = 30$). By contrast, Group VI ($n = 80$) and Group IV ($n = 60$) demonstrate the lowest pooling factor values and therefore are closer to the no-pooling estimates. Interestingly, the consideration of group-specific variances with the first three hierarchical formulations allowed greater flexibility and thus more distinct excursions of the group-specific parameter estimates from the grand means regardless of the corresponding sample size (Table 3), such as the values of the *k* coefficient in Groups I (1.53 ± 0.37 year$^{-0.55}$), V (0.81 ± 0.19 year$^{-0.66}$), and VII (0.95 ± 0.39 year$^{-0.39}$), and the *x* power in the Groups II (0.26 ± 0.11), and VII (0.39 ± 0.21).

According to the phosphorus loading model used, the *TP* loss rate is approximately proportional to the inverse of the lake hydraulic retention time, and our exercise also renders support to the Cheng et al.'s (2010) finding that the nature of the $\sigma - 1/\tau_w$ relationship varies significantly with the morphological/hydraulic characteristics of the lakes. Specifically, the slope of this relationship is steeper in shallow lakes ($k = 1.53 \pm 0.37$ year$^{-0.55}$) as well as in lakes with intermediate depth ($1.65\ \text{m} \leq \bar{z} \leq 10.3$ m) and surface area ($1.47\ \text{km}^2 \leq A \leq 20.3\ \text{km}^2$) along with hydraulic retention time shorter than 0.17 years ($k = 1.23 \pm 0.50$ year$^{-0.45}$) (Table 3). By contrast, the relationship is somewhat weaker in lakes with large surface area (>20.3 km^2) and intermediate depth ($k = 0.81 \pm 0.19$ year$^{-0.66}$), and deep lakes with hydraulic retention time between 9.8 years and 17.8 years ($k = 0.95 \pm 0.39$ year$^{-0.39}$). In a similar manner, our results verify the conclusions of other studies that the *TP* sedimentation rate is best approximated as being proportional to the inverse square root of τ_w, i.e., $\sigma \approx {\tau_w}^{-0.53}$ (see also Fig. 2b in Ahlgren et al., 1988). However, we also found that the same relationship can vary from a power of 0.26, in lakes with mean depth between 1.65 m and 10.3 m and surface area lower than 1.47 km^2, to a power of 0.76, in lakes of intermediate depth ($1.65\ \text{m} \leq \bar{z} \leq 10.3$ m) and surface area ($1.47\ \text{km}^2 \leq A \leq 20.3\ \text{km}^2$) with hydraulic retention time longer than 0.17 years.

Based on the posterior parameter patterns, lakes with intermediate depths and large surface areas demonstrate phosphorus loss rates of 0.32 to 5.0 year^{-1} (Group V) across the range of hydraulic retention times τ_w (<0.007–12.7 years) recorded in our dataset. Along the same line of thinking, we can infer that the median sedimentation rates vary from 0.79 to 41.2 year^{-1} in very shallow lakes (Group I). In the same context though, the relatively poor model performance reinforces the scepticism about the applicability of the "conventional" phosphorus loading models with the latter type of lakes (Jensen et al., 2006; Nürnberg and LaZerte, 2004). Several studies advocate the notion that some of the underlying assumptions (e.g., steady state, first-order losses) should be revisited and other unaccounted factors affecting the efficiency of *TP* retention need to be explicitly considered. For example, the lack of stratification during extended periods in the summer and the tight water column–sediment coupling are predominant features of the shallow water bodies (Scheffer, 2004). In shallow systems, the sediment surface to water volume ratio is high, and therefore the intense sediment–water column interplay aggravates the eutrophication problem, leading to a considerable time lag in their response to the reduction of external nutrient loading (Søndergaard et al., 2003). Sediment resuspension, driven by both bioturbation and wind action, is responsible for a substantial nutrient reflux rates into the water column. Likewise, the elevated amount of phosphorus retained in the sediments is subject to diagenesis processes and gets mobilized to the interstitial waters as phosphate, subsequently returning into the water column through Fickian diffusive transport (Søndergaard et al., 2003). Many of the associated sediment processes (e.g., bacteria-mediated mineralization) also display seasonal variation, with their maximal rates typically observed during the summer period when the highest water temperatures occur (Søndergaard et al., 2003). Hence, while the improvement brought about by the eight-group hierarchical configuration is certainly encouraging, the multitude of transient dynamics that typically characterize the shallow systems invites building more realism into

Table 3
Lake phosphorus loading model: summary statistics of the posterior parameter distributions for the four hierarchical model configurations founded upon the eight groups delineated from the Cheng et al. (2010) CART analysis.

	Model 1 — classical		Model 2 — informative prior		Model 3— alternative error		Model 4 — multivariate normal		Model 5 — multivariate normal & alternative error	
	Mean	SD	Mean	SD	Mean	SD	Mean	SD	Mean	SD
k_1	1.53	0.37	1.52	0.37	1.49	0.38	1.29	0.24	1.23	0.24
k_2	1.01	0.19	1.02	0.19	0.95	0.19	1.06	0.17	0.98	0.17
k_3	1.23	0.5	1.23	0.52	1.19	0.52	1.13	0.25	1.08	0.25
k_4	1.05	0.14	1.05	0.14	1.03	0.14	1.08	0.13	1.06	0.13
k_5	0.81	0.19	0.81	0.19	0.79	0.19	0.91	0.17	0.88	0.17
k_6	1.16	0.13	1.16	0.13	1.10	0.13	1.15	0.12	1.09	0.12
k_7	0.95	0.39	0.96	0.39	0.91	0.39	1.01	0.28	0.96	0.27
k_8	1.16	0.36	1.17	0.36	1.09	0.34	1.11	0.23	1.05	0.23
x_1	0.55	0.17	0.55	0.17	0.56	0.18	0.49	0.14	0.5	0.15
x_2	0.26	0.11	0.26	0.12	0.28	0.13	0.31	0.11	0.33	0.12
x_3	0.45	0.19	0.44	0.17	0.47	0.19	0.43	0.13	0.45	0.14
x_4	0.76	0.13	0.76	0.13	0.78	0.13	0.7	0.12	0.7	0.12
x_5	0.66	0.16	0.65	0.17	0.66	0.17	0.58	0.13	0.59	0.13
x_6	0.45	0.09	0.45	0.09	0.49	0.10	0.46	0.09	0.49	0.09
x_7	0.39	0.21	0.38	0.2	0.41	0.21	0.36	0.14	0.38	0.14
x_8	0.5	0.08	0.5	0.08	0.51	0.09	0.51	0.06	0.51	0.07
k	1.09	0.17	1.09	0.15	1.04	0.18	1.09	0.14	1.04	0.14
x	0.51	0.13	0.49	0.12	0.52	0.13	0.48	0.09	0.49	0.09
σ_{k1}	0.56	0.83	0.54	0.45	0.55	0.52				
σ_{k2}	0.39	0.29	0.39	0.28	0.40	0.30				
σ_{k3}	0.48	0.45	0.47	0.49	0.48	0.48				
σ_{k4}	0.39	0.29	0.38	0.29	0.39	0.31				
σ_{k5}	0.44	0.37	0.45	0.38	0.44	0.34				
σ_{k6}	0.39	0.28	0.38	0.28	0.39	0.30				
σ_{k7}	0.45	0.35	0.46	0.36	0.46	0.38				
σ_{k8}	0.43	0.34	0.43	0.32	0.43	0.34				
σ_{x1}	0.39	0.29	0.39	0.28	0.39	0.29				
σ_{x2}	0.42	0.3	0.41	0.3	0.42	0.33				
σ_{x3}	0.39	0.29	0.39	0.28	0.39	0.28				
σ_{x4}	0.43	0.32	0.43	0.38	0.43	0.32				
σ_{x5}	0.4	0.31	0.4	0.3	0.40	0.31				
σ_{x6}	0.37	0.24	0.38	0.27	0.38	0.29				
σ_{x7}	0.4	0.29	0.4	0.29	0.40	0.32				
σ_{x8}	0.38	0.3	0.37	0.29	0.37	0.28				
σ_k	0.5	0.55	0.38	0.27	0.51	0.74	0.25	0.11	0.24	0.11
σ_x	0.49	0.54	0.36	0.23	0.49	0.69	0.21	0.07	0.21	0.07
σ_{kx}							−0.01	0.04	−0.004	0.036
μ_k	1.16	0.66	1.12	0.08	1.14	0.79				
μ_x	0.67	0.62	0.47	0.04	0.68	0.72				
σ	0.5	0.02	0.5	0.02			0.51	0.02		
φ_1					2.96	2.51			3.17	2.49
φ_0					1.28	0.11			1.27	0.11

the phosphorus loading models. It seems unlikely that a steady state model, originally developed to support predictions on an annual scale, will capture biogeochemical processes occurring in shorter time scales.

Lakes with intermediate mean depths and small surface areas (Group II) display a very wide range of sedimentation rates, 0.35 to 283 year^{-1}, depending on the prevailing hydraulic loading conditions ($5.5 \cdot 10^{-4}$ — 4.1 years). Likewise, lakes with mean depths and surface areas lying at intermediate values are projected to experience sedimentation rates of 3.36–45.6 year^{-1} and 0.64–1.57 year^{-1}, if their average hydraulic retention time is shorter (Group III) or longer (Group IV) than 0.17 years, respectively. In a similar manner, deep lakes with hydraulic retention time shorter than 9.8 years (Group VI) are characterized by sedimentation rates of 0.35 to 12.8 year^{-1}. Further increase of the residence time in deep lakes (Group VII) leads to a decline of the sedimentation rates (0.15–0.20 year^{-1}) and ultimately results in fairly low sedimentation rates (0.04 to 0.26 year^{-1}), when very low flushing rates are experienced (*Group VIII*). Generally, the higher sedimentation rates in lakes with short hydraulic retention times over the rates calculated for longer retention times reinforces the well-documented positive relationship between *TP* loss and lake flushing rates (Ahlgren et al., 1988). This counterintuitive relationship was attributed to the fact that the former lakes usually receive relatively greater inputs of allochthonous, mineral-bound (and thus more susceptible to settling) particulate phosphorus than do the latter ones (Canfield and Bachmann, 1981; Schindler et al., 1978). In addition, although deep waters are generally less turbulent than surface waters which increases particle aggregation and consequently the effective settling velocity of particulate matter (Malmaeus and Håkanson, 2004), the predicted pattern of lower *TP* loss rates in the latter group of lakes emphasizes the capacity of in-lake processes (mineralization, uptake) to increase the nutrient retention time in the water column.

On a final note, we should always bear in mind that Vollenweider-type models predict steady-state outcomes, although lakes are subject to considerable year-to-year variations and therefore steady-state conditions can only be approximated with long-term averages. The present analysis was based on systems that were not experiencing transient dynamics, after the implementation of phosphorus loading reduction strategies, and were studied from one year to several decades (Brett and Benjamin, 2008). However, models based on studies of small lakes that last less than 5–7 years are less likely to predict long-term averages accurately, because of the pronounced effect that extreme years can have. Even when steady-state models are parameterized with more than 5 years worth of data, there is always an increased likelihood that a given year is not close to the long-term mean. Inter-annual variation in runoff can affect residence time, a key predictor variable, much more in

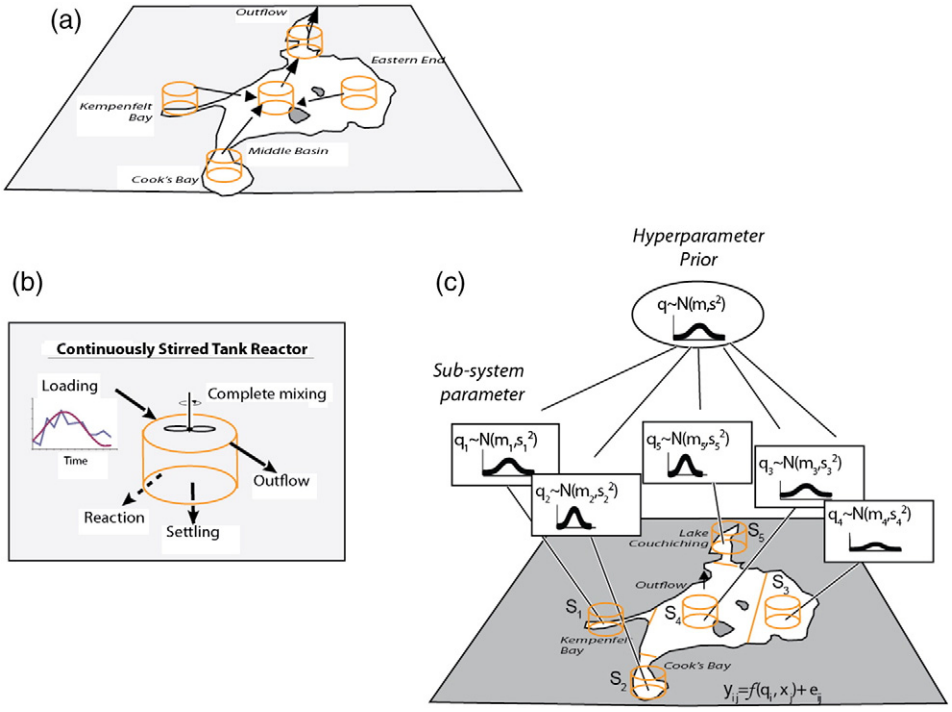

Fig. 2. Spatial segmentation (*a*) and basic concepts (*b*) of the continuously-stirred-talk reactor (CSTR) model, forced with idealized sinusoidal loading, to predict total phosphorus concentrations in Lake Simcoe, Ontario, Canada. (c) Hierarchical configuration of the phosphorus loading model for Lake Simcoe.

small than in large systems, and this could be another plausible explanation for the higher error typically found with the former group of lakes.

3.2. How effectively can we accommodate the seasonality and spatial heterogeneity of phosphorus dynamics within a single large lake?

Striving for an improvement of the existing lake eutrophication models, the Bayesian hierarchical proposition may be useful when modelling large systems, where the most degraded areas are nearshore zones above the summer thermocline adjacent to the mouths of large rivers and/or semi-enclosed embayments with restricted mixing with offshore waters. In this regard, Zhang and Arhonditsis (2009) questioned to what extent this type of spatial heterogeneity can be fully accommodated by spatially-explicit, process-based models with common parameter values over the entire system; that is, how realistic is to assume that the same sedimentation rate (a surrogate of a suite of physical, chemical, and biological processes) characterizes the entire waterbody? The practical compromise between entirely site-specific and globally-common parameter estimates offered by the hierarchical approach may be a conceptually more sound strategy. Here, we evaluate a novel phosphorus loading model that is founded upon two basic augmentations: (*i*) *TP* spatial patterns are accommodated by location-specific sedimentation rates; and (*ii*) *TP* dynamics within each location are primarily modulated by the seasonal variability of the external phosphorus loading. Lake Simcoe is an excellent case study to examine the model due to its distinct morphological characteristics of embayments, as the adoption of a single-box, steady state approach will not offer the capacity to reproduce the considerable intra-annual variability of the inshore locations, while a multi-box strategy with lakewide parameters may be inadequate to shed light on their interplay with the central segments of the lake (Gudimov et al., 2012). Importantly, probability distributions with known mean and variances are used to reproduce the year- and segment-specific phosphorus loading (Fig. 3) and flushing rates (Fig. 4), and thus the error of the corresponding estimates is propagated through the model.

The application of the *TP* model provided satisfactory fit to the measured *TP* concentrations in the five segments considered, resulting in *RMSE* values lower than 5 μg *TP* L^{-1} (Fig. 5). The main exception was the segment that represents the Cook's Bay (*RMSE* = 6.87 μg *TP* L^{-1}), which is also consistently characterized by the highest *TP* levels in the system (18.4 ± 7.7 μg *TP* L^{-1}). The second highest model error was recorded in the Main Basin (*RMSE* = 4.95 μg *TP* L^{-1}), while the rest three segments were characterized by *RMSE* values lower than 4 μg *TP* L^{-1}. Given the aforementioned assumption that the segment-specific *TP* dynamics are mainly driven by the seasonal variability of exogenous loading, our model predicts that the inflowing *TP* loads alone can indeed induce significant oscillatory behaviour in Cook's Bay. However, the discrepancy between observed and predicted concentrations partly stems from the fact that the postulated phase shifts, $\varphi_{(ij)}(\omega)$, cannot fully capture the evolution of ambient *TP* levels in the system. The predicted *TP* dynamics in larger and/or offshore segments were also significantly muted, indicative of a more complex interplay among exogenous loading, hydrodynamics, and biological productivity that most likely modulates in-lake *TP* variability. In particular, we note that the coarser representation of Kempenfelt Bay of the present study relative to Gudimov et al.'s (2012) segmentation (i.e., one instead of three spatial compartments) profoundly understated the observed intra-annual phosphorus variability.

All the posterior estimates of the segment- and year-specific net *TP* loss rates, κ_{2tj}, were well-identified and independent from the corresponding estimates of the flushing (or net exchange) rates (see also Fig. 3 in the Supporting Information of Gudimov et al., 2012). The sedimentation rates demonstrated significant year-to-year and among-segment variability (Table 4). Not surprisingly, the highest sedimentation rates were estimated in Cook's Bay (i.e., from 2.125 ± 0.546 $year^{-1}$ to 4.810 ± 0.854 $year^{-1}$) and Kempenfelt Bay (i.e., from 0.800 ± 0.302 $year^{-1}$ to 2.216 ± 0.711 $year^{-1}$). Given that both embayments are located in the vicinity of major tributary outlets, there are several plausible explanations for this distinct behaviour relative to rest of the lake: (*i*) both spatial compartments constitute transitional zones that regulate the fate and transport of external phosphorus loadings to the deeper parts of the lake; (*ii*) the presence of dreissenids that have the capacity to filter suspended particles from the water column, thereby exerting significant control of the ambient *TP*; and (*iii*) the

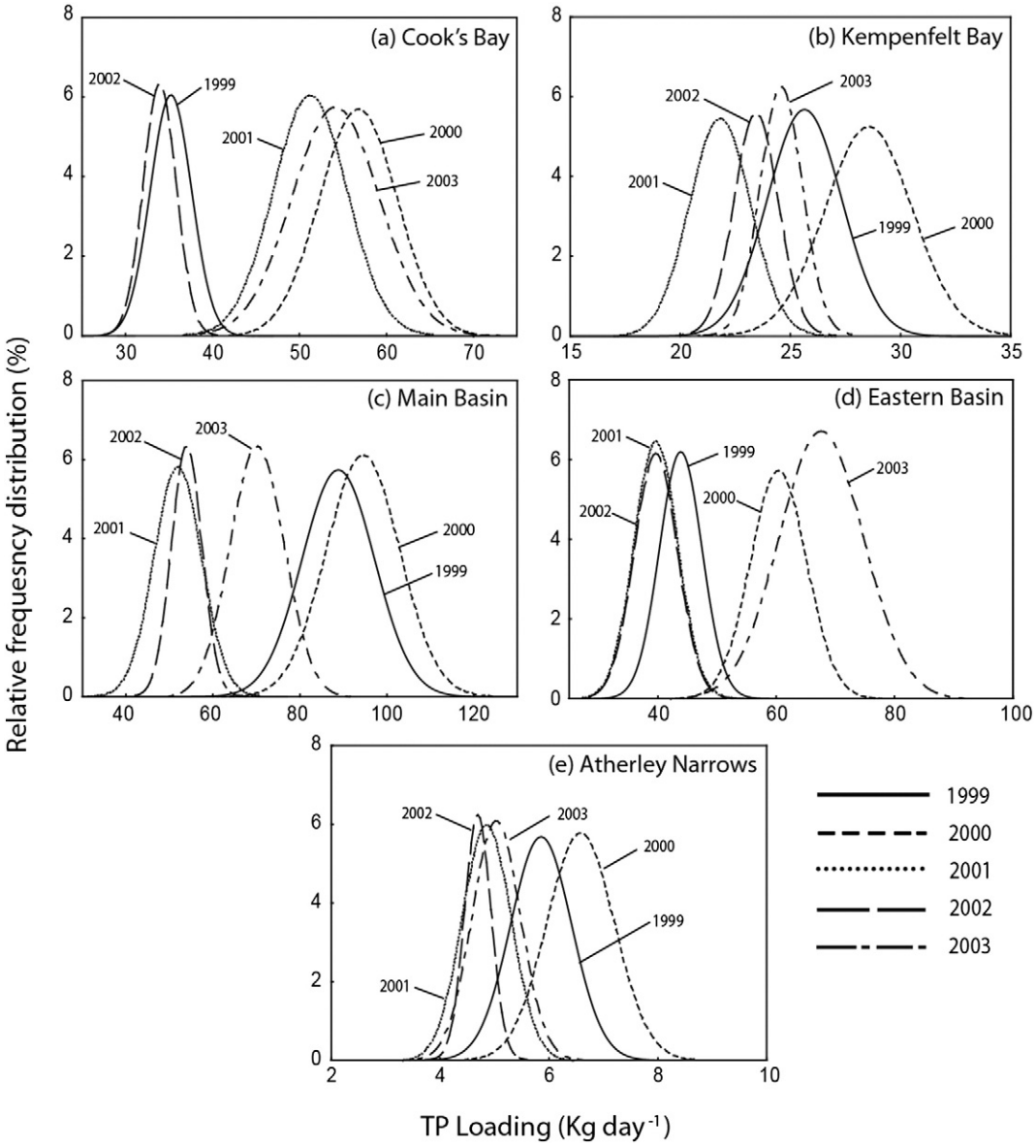

Fig. 3. Posterior predictive distributions of annual TP loading (tonnes year^{-1}) in each segment of Lake Simcoe; (*a*) Cook's Bay, (*b*) Kempenfelt Bay, (*c*) Main Basin, (*d*) Eastern Basin, and (*e*) Atherley Narrows.

excessive macrophyte growth that capitalizes upon the favourable environment of Cook's Bay (i.e., shallower depths, elevated nutrient levels, increased water clarity, and fine-grained sediments) and act as a net sink of the *TP* pool in the water column (Dittrich et al., 2013; Gudimov et al., 2015). Consistent with the previously reported identifiability patterns, the segment-specific standard error values of the sedimentation rates ($\sigma_{\kappa 2j}$) were also well delineated, reflecting the significant year-to-year variability in Cook's Bay (3.408 year^{-1}) and Kempenfelt Bay (1.152 year^{-1}) relative to the other three segments (<0.345 year^{-1}).

Generally, the posterior estimates of the sedimentation and outflow rates suggest that a significant portion of the annual *TP* inputs from the Holland River in Cook's Bay (≈380 mg m^{-2} year^{-1}) is lost (295 mg m^{-2} year^{-1}) in the sediments or in the hypolimnion of the outer Bay, while a lower fraction (85.7 mg m^{-2} year^{-1}) is transported horizontally to the Main Basin (Fig. 6). Likewise, more than half of the *TP* loads (≈255 mg m^{-2} year^{-1}) in Kempenfelt Bay are subjected to sedimentation (149.2 mg m^{-2} year^{-1}) and the remaining amount of phosphorus is transferred to the central area of the lake (105.8 mg m^{-2} year^{-1}). Relative to our posterior net sedimentation rates, Hiriart-Baer et al. (2011) recently reported post-1970 estimates of the gross *TP* accumulation in Cook's Bay and Kempenfelt Bay sediments at the level of 250–750 mg *P* m^{-2} year^{-1} and 300 mg *P* m^{-2} year^{-1}, respectively. The two-fold difference between gross and net *TP* sedimentation rates could be interpreted as a support to our earlier point that a suite of ecological factors and feedback loops, such as macrophyte growth, dreissenids activity, sediment resuspension and *P* release determine the fate and transport of phosphorus in the two embayments. The net areal sedimentation rate in the Main Basin was nearly twice (94.46 mg m^{-2} year^{-1}) as high as the values predicted in the Eastern Bain and the Atherley Narrows (41.07 to 52.01 mg m^{-2} year^{-1}). It is also worth noting that the average areal loading in the latter three segments ranged from 64.73 mg m^{-2} year^{-1} (Eastern Basin) to 94.46 mg m^{-2} year^{-1} (Main Basin). The annual *TP* outflows from Atherley Narrows were estimated at an average level of 289 mg m^{-2} years^{-1} (or 9.3 tonnes year^{-1}), and the *TP* retention fraction varied from 85% to 93%; both values are consistent with existing estimates independently calculated from *TP* mass balance budgets for Lake Simcoe (Young et al., 2011).

The proposed phosphorus loading model, comprising a feedforward series of completely mixed reactors, is a pragmatic approach to

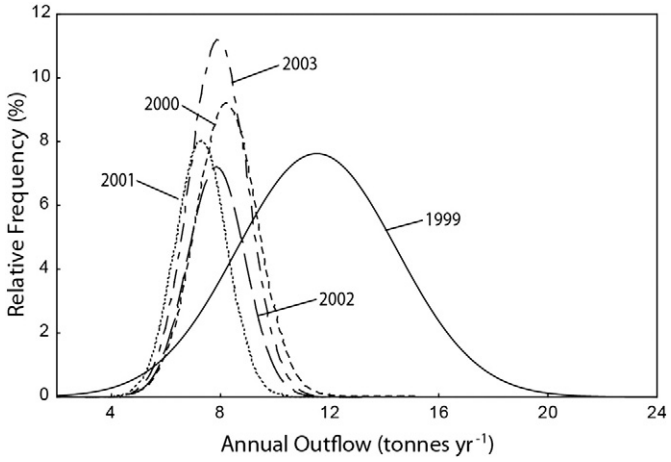

Fig. 4. Posterior predictive distributions of TP outflow rates (tonnes year^{-1}) at the outlet of Lake Simcoe (Atherley Narrows) during the examined period (1999–2003).

accommodate the spatial variability in Lake Simcoe, given the lack of consistent chloride measurements to properly constrain the intersegment mixing processes during the study period. This approach is conceptually suitable to model horizontal mass exchanges in a chain of lakes or a stream, and Gudimov et al. (2012) showed that its credibility to accommodate the spatial heterogeneity within a single lake is limited under certain conditions. One instance is when wind-induced circulation patterns negate the pre-specified unidirectional flow, and thus the model fails to account for the dilution effect of the predominant inflows of water masses from the outer lake into the two embayments [See Gudimov et al.'s (2012) Supporting Information]. A second problematic facet of the model is the large spatial compartment representing the eastern basin, in which the estimated net outflow rates are fairly low (relative to its volume) and therefore the model postulates that the inflowing *TP* loads from the watershed are subject to prolonged sedimentation. As a post-hoc exercise, we here examine Gudimov et al.'s (2012) hypothesis that this simplification could potentially lead to an overestimation of the sedimentation rates, when the corresponding segment receives substantial exogenous loads and/or is characterized by a distinct *TP* concentration gradient. The phosphorus loading model was calibrated under two alternative scenarios of low (present average values) and high (present average values increased by 10 μg L^{-1}) *TP* concentrations in the Eastern Basin and we subsequently compared the annual phosphorus fluxes and sedimentation rates. The posterior statistics suggest that the characterization of the phosphorus cycle with the present model unidirectional construct is fairly robust and (Table S2 & Fig. S2). Counter to Gudimov et al.'s (2012) assertions though, the sedimentation fluxes in the Eastern Basin were somewhat reduced and instead the model posteriors are indicative of higher net *TP* export into the Main Basin and enhanced settling rates in the latter segment (Fig. S2). This model projection is consistent with Gudimov et al.'s (2015) conceptualization that pinpoints the close association of the energy and nutrient subsidies from the littoral zone, stemming from both allochthonous and autochthonous sources, with the broader ecosystem functioning, potentially mediated by the particular morphological features and hydrodynamic patterns of Lake Simcoe.

4. Conclusions

In this study, we revisited the predictive capacity of phosphorus loading models using a Bayesian hierarchical framework. These models offer a first-principles approach to assist the decision-making process and potentially facilitate lake management actions in space and time (Brett and Benjamin, 2008; Chapra and Dolan, 2012; Cheng et al., 2010; Stow et al., 2014). The Bayesian hierarchical proposition is a compromise between site-specific (where limited local data is a problem) and globally-common (where heterogeneous systems in wide geographical areas are assumed to be identical) parameter estimates. Under the hierarchical structure, the models are dissected into levels (hierarchies) that explicitly account for the role of significant sources of variability, e.g., geographical location, trophic status, morphometry,

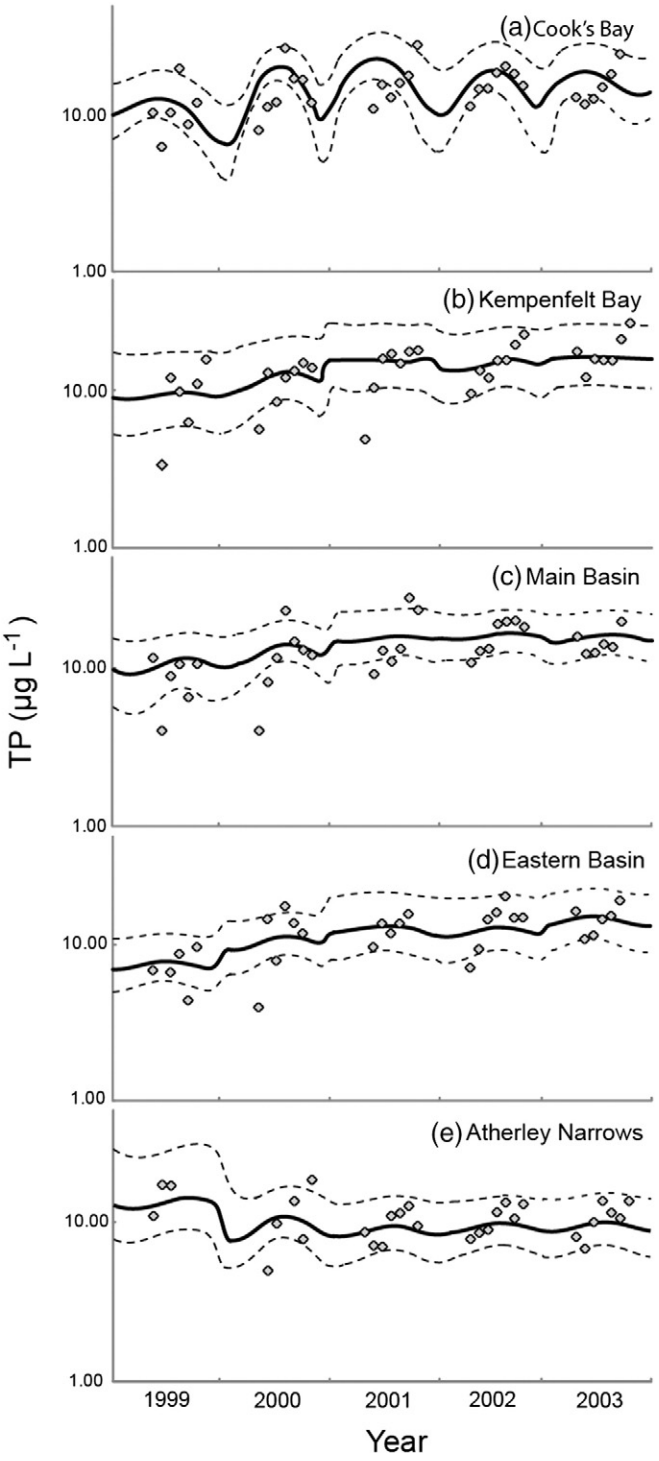

Fig. 5. Comparison of the observed versus mean predicted (along with 95% credible intervals) total phosphorus concentrations in each segment of Lake Simcoe; (*a*) Cook's Bay, (*b*) Kempenfelt Bay, (*c*) Main Basin, (*d*) Eastern Basin, and (*e*) Atherley Narrows.

Table 4
Continuously stirred tank reactor model: Summary statistics of the posterior parameter distributions for the five segments in Lake Simcoe.

	Cook's Bay		Kempenfelt Bay		Main Basin		Eastern Basin		Atherley Narrows	
Parameters	Mean	SD	Mean	SD	Mean	SD	Mean	SD	Mean	SD
$\kappa_{2(1999j)}$	3.283	0.688	2.216	0.711	1.026	0.209	0.785	0.148	0.664	0.276
$\kappa_{2(2000j)}$	4.810	0.854	1.929	0.575	1.070	0.188	0.766	0.140	0.655	0.268
$\kappa_{2(2001j)}$	2.947	0.676	0.800	0.302	0.578	0.110	0.362	0.097	0.661	0.263
$\kappa_{2(2002j)}$	2.125	0.546	0.994	0.327	0.533	0.094	0.376	0.094	0.650	0.261
$\kappa_{2(2003j)}$	3.683	0.840	0.930	0.312	0.712	0.122	0.613	0.128	0.657	0.256
$\sigma_{\kappa 2j}$	3.408	1.506	1.152	0.6938	0.3453	0.2078	0.2933	0.1627	0.2311	0.2198
τ					0.327, 0.025					
κ_2					0.683, 0.118					
$\kappa_{2\mu}$					10.70, 25.70					
$\sigma_{\kappa 2}$					53.37, 645.4					

mixing regime, or even watershed land use patterns. The major lessons learned from our exercise are as follows:

- Consistent with Ahlgren et al.'s (1988) assertion, the present analysis provides evidence that the delineation of more homogeneous subsets of data can indeed give models with better predictive value. The eight-node configuration has led to a distinct model performance improvement, founded upon well-identified posterior parameter estimates that allow drawing meaningful large-scale patterns.
- A second key finding from our analysis is that the application of phosphorus loading models to shallow lakes has limited learning capacity, even with the coarse annual resolution of the "Vollenweider-type" models, as some of the underlying assumptions (e.g., steady state, first-order losses) may not hold true. Further improvements with the modelling of shallow lakes can only be obtained if several potentially important ecological factors and feedback loops are explicitly considered.
- The group-level posterior patterns are robust to the different assumptions/complexity levels of the hierarchical framework used, although the degree of specificity of the parameter estimates depends on the sample size of the corresponding group.
- The characterization of the model structural error as function of the inflow weighted *TP* concentration was intended to offer a lake-specific characterization of the model inadequacy relative to the typically used global specifications. While this strategy led to a model improvement in the oligo- and mesotrophic systems included in our dataset, the postulated rectangular hyperbolic pattern evidently inflates the error when applied to the eutrophic end of the lake spectrum. The identification of the optimal relationship between the residual model variability and the potential explanatory variables could be a meaningful follow-up exercise.
- Recognizing its conceptual limitations, the feedforward series of completely mixed reactors combined with a Bayesian hierarchical calibration framework offers a first approximation of the spatial variability in cases where we have evidence that the single-box approach is an oversimplification. Our example with the Lake Simcoe application showed that the derived sedimentation rates as well as the characterization of the phosphorus fate and transport are on par with existing empirical evidence from the system.
- The assumption that phosphorus dynamics in a particular location are primarily shaped by the seasonal variability of the adjacent external phosphorus loading cannot consistently reproduce the temporal patterns in large lakes. Unless the grid resolution is appropriately refined, the proposed scheme is likely inadequate to reproduce the suite of mechanisms underlying the intra-annual lake variability; especially in offshore areas.

The tendency to invoke complexity as a means for improving the learning capacity of our models is primarily prompted by the need to address environmental management problems that often involve complex policy decisions. Problems related to eutrophication, biodiversity, fisheries management, habitat conservation and restoration, and ultimately sustainable economic development are often supported by complex ecosystem models. However, our ability to properly constrain the inputs of such modelling constructs from existing empirical knowledge and data is limited, and thus the resulting poor identifiability undermines their credibility as management tools. In this context, we believe

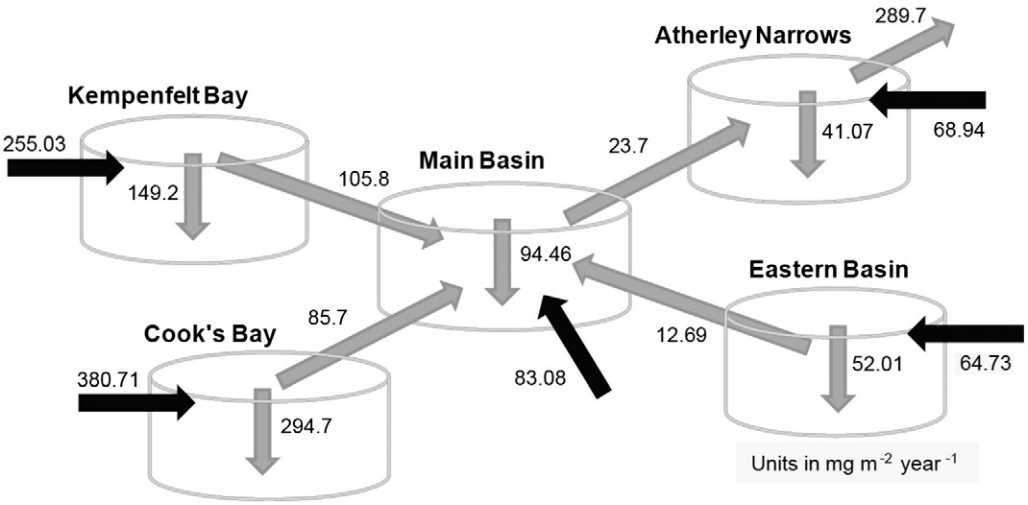

Fig. 6. Areal average *TP* sources, sinks, and transport (mg m^{-2} $year^{-1}$) among the spatial segments in Lake Simcoe.

that lake modellers should cherish the role of phosphorus loading models, as they offer adequate first approximations until simplicity can be gradually traded for increased explanatory power. In this study, we highlight the benefits of simple models that remain within the bounds of data-based parameter estimation and therefore can undergo rigorous error analysis. The Bayesian hierarchical approach offers an appealing ad-hoc strategy to gradually increase model complexity and subsequently enhance their mechanistic underpinning, whenever possible and relevant.

Acknowledgements

Funding for this study was provided by the National Sciences and Engineering Research Council of Canada (NSERC) (#482601) through a Doctoral Graduate Scholarship (Yuko Shimoda) and a Discovery Grant (George Arhonditsis). All the material pertinent to this study is available upon request from the corresponding author.

Appendix A. Terminology and notation of the models examined in this analysis

Lake phosphorus model: The foundation for predicting the total phosphorus concentrations in lakes was first proposed by Vollenweider (1969) with his mass-balance model. Under steady state conditions, this model is expressed as:

$$\mathrm{TP}_{\mathrm{lake}} = \frac{L}{\bar{z}(\rho+\sigma)}.$$

This relationship is mathematically equivalent to the classic model from chemical engineering relating input and output concentrations of a substance that undergoes a first-order decay reaction in a continuous flow stirred tank reactor (Higgins and Kim, 1981; Brett and Benjamin, 2008):

$$\mathrm{TP}_{\mathrm{lake}} = \frac{\mathrm{TP}_{\mathrm{in}}}{1+\sigma\tau_w}.$$

If we assume that $\sigma = k{\tau_w}^{x-1}$, where k and x are adjustable parameters, then the model becomes:

$$\mathrm{TP}_{\mathrm{lake}} = \frac{\mathrm{TP}_{\mathrm{in}}}{1+k\tau_w^{\mathrm{x}}}$$

TP_{lake}	*TP* concentration in the lake and its outflow (μg L^{-1})
TP_{in}	inflow weighted *TP* concentration (μg L^{-1})
L	areal *TP* loading rate (mg *TP* m^{-2} $year^{-1}$), $L = (Q \times TP_{in})/A_L$
σ	first-order rate coefficient for *TP* loss (or sedimentation) from the lake (yr^{-1})
$\bar{z}$	mean lake depth (m), $\bar{z} = V/A_L$
A_L	lake surface area (m^2), $A_L = V/\bar{z}$
V	lake volume (m^3), $V = A_L \times \bar{z}$
τ_w	mean hydraulic retention time (yr), $\tau_w = 1/\rho = Q/V$
ρ	flushing rate (yr^{-1}), $\rho = 1/\tau_w = V/Q$
q_s	areal hydraulic loading (m yr^{-1}), $Q/A_L = \rho \times \bar{z} = \bar{z}/\tau_w$
Q	hydraulic inflow rate (m^3 $year^{-1}$), $Q = q_s \times A_L = V/\tau_w = V \times \rho$.

Continuously stirred tank reactor model forced with sinusoidal loading:

W_{avg}	mean loading entering each segment (tonnes day^{-1})
$W_{amplitude}$	amplitude around the mean loading (tonnes day^{-1})
λ	total loss rate (day^{-1}), where $\lambda = Q/V + k + \nu/H$, $\kappa_1 = Q/V$, and $\kappa_2 = k + \nu/H$
Q	volumetric flow rate water sources entering each segment (m^3 day^{-1})
V	volume of system (m^3)
k	first-order decay rate (day^{-1})
ν	first-order settling rate (m day^{-1})
H	mean depth of each segment (m)
θ	phase shift (radians)
$\varphi(\omega)$	additional phase shift (radians) that is a function of the frequency
ω	angular frequency of oscillation (radians day^{-1}), $\omega = 2\pi/T$
T	period of the oscillation (day)
i	year
t	Julian day of year i.

Spatial segmentation of model:

j	segments that do not have antecedent spatial compartments (Cook's Bay, Kempenfelt Bay and Eastern Bay)
k	segment that receives pollutants from adjacent segments (Main Basin)
l	segment that receives pollutants from segment k and exports them out of the system via outflows (Atherley Narrows).

Appendix B. Bayesian parameter estimation for the hierarchical cross-system *TP* model

Using the notation in Section 2.1 and Appendix A, the likelihood function for the hierarchical model is:

$$\begin{aligned} L(y|x,\ \Sigma_\theta,\ \mu,\ \Sigma_\mu,\ \tau^2) &= L(y|x,\ \theta',\ \tau^2)L(\theta'|\theta,\ \Sigma_\theta)L(\theta|\mu,\ \Sigma_\mu) \\ &= \left(\frac{1}{2\pi\tau^2}\right)^{\frac{N}{2}} \exp\left(-\frac{1}{2\tau^2}\sum_{j=1}^{m}\sum_{i=1}^{n_j}\left[y_{ij}-f(x_{ij},\theta_j)\right]^2\right) \\ &\quad \times \prod_{j=1}^{m}\left(\frac{1}{2\pi\sqrt{|\Sigma_{\theta j}|}}\right)\exp\left(-\frac{1}{2}\sum_{j=1}^{m}(\theta_j-\theta)^T\Sigma_{\theta j}^{-1}(\theta_j-\theta)\right) \\ &\quad \times \frac{1}{2\pi\sqrt{|\Sigma_\mu|}}\exp\left(-\frac{1}{2}(\theta-\mu)^T\Sigma_\mu^{-1}(\theta-\mu)\right) \text{ with } N=\sum_{j=1}^{m}n_j \end{aligned}$$

where y = in-lake *TP* concentrations used to update the model; m = number of lake types considered by the hierarchical model; n_j = number of lakes in lake type j; x = model inputs with x_{ij} the vector $[TP_{in}, \tau_w]$ for lake i in group j; $\theta' = [\theta_1, \theta_2, \ldots, \theta_j]$ with θ_j = vector of parameters $[k_j, x_j]$ in lake type j; θ = vector of global parameters $[k, x]$; μ = vector of hyperparameters $[k_\mu, x_\mu]$; $\Sigma_{\theta j} = \begin{bmatrix} \sigma_{kj}^2 & 0 \\ 0 & \sigma_{xj}^2 \end{bmatrix}$; $\Sigma_\mu = \begin{bmatrix} \sigma_k^2 & 0 \\ 0 & \sigma_x^2 \end{bmatrix}$; and τ^2 is the model error variance;The posterior of the classical hierarchical model is:

$$\begin{aligned} \pi\left(\theta', \theta, \Sigma_\theta, \mu, \Sigma_\mu, \tau^2|x,y\right) &= L\left(y|x,\ \theta',\ \tau^2\right)L\left(\theta'|\theta,\ \Sigma_\theta\right)L(\theta|\mu,\ \Sigma_\mu)\pi(\Sigma_\theta, \mu, \Sigma_\mu, \tau^2) \\ &= \left(\frac{1}{2\pi\tau^2}\right)^{\frac{N}{2}} \exp\left(-\frac{1}{2\tau^2}\sum_{j=1}^{m}\sum_{i=1}^{n_j}\left[y_{ij}-f(x_{ij},\theta_j)\right]^2\right) \\ &\quad \times \prod_{j=1}^{m}\left(\frac{1}{2\pi\sqrt{|\Sigma_{\theta j}|}}\right)\exp\left(-\frac{1}{2}\sum_{j=1}^{m}(\theta_j-\theta)^T\Sigma_{\theta j}^{-1}(\theta_j-\theta)\right) \\ &\quad \times \frac{1}{2\pi\sqrt{|\Sigma_\mu|}}\exp\left(-\frac{1}{2}(\theta-\mu)^T\Sigma_\mu^{-1}(\theta-\mu)\right) \\ &\quad \times \prod_{j=1}^{m\times\kappa}\frac{\beta_j^{\alpha j}}{\Gamma(\alpha_j)}\left(\sigma_j^2\right)^{-\alpha_j-1}\exp\left(-\frac{\beta_j}{\sigma_j^2}\right) \\ &\quad \times \frac{1}{2\pi\sqrt{|\Sigma_0|}}\exp\left(-\frac{1}{2}(\mu-\mu_0)^T\Sigma_0^{-1}(\mu-\mu_0)\right) \\ &\quad \times \frac{\beta_0^{\alpha_0}}{\Gamma(\alpha_0)}\left(\sigma^2\right)^{-\alpha_0-1}\exp\left(-\frac{\beta_0}{\sigma^2}\right) \\ &\quad \times \frac{\beta^{\alpha}}{\Gamma(\alpha)}\left(\tau^2\right)^{-\alpha-1}\exp\left(-\frac{\beta}{\tau^2}\right) \end{aligned}$$

where $\mu_0 = [0, 0]$; $\Sigma_0 = \begin{bmatrix} 10000 & 0 \\ 0 & 10000 \end{bmatrix}$; α, α_0, α_j = the shape parameters for the inverse gamma distributions assigned to model error

variance, global, and group-specific parameter variance terms, respectively; κ = the dimension of θ_j or number of model parameters (=2) and β, β_0, β_j = the scale parameters for the inverse gamma distributions assigned to the model error variance, global, and group-specific parameter variance terms.

The posterior of the hierarchical model with alternative model structural error is:

$$\begin{aligned}
&\pi\left(\theta', \theta, \Sigma_\theta, \mu, \Sigma_\mu, \varphi, \Sigma_\varphi | x, y\right) = L(y|x, \theta', \varphi, \Sigma_\varphi) L\left(\theta' | \theta, \Sigma_\theta\right) L(\theta|\mu, \Sigma_\mu) \pi(\Sigma_\theta, \mu, \Sigma_\mu, \varphi, \Sigma_\varphi) \\
&= \left(\frac{1}{2\pi}\right)^{\frac{N}{2}} \left(exp\left(\sum_{j=1}^{m}\sum_{i=1}^{nj}\left(\varphi_0 + \varphi_1\left(\frac{1}{TP_{in(ij)}}\right)\right)\right)\right)^{\frac{1}{2}} \\
&\quad \times exp\left(-\sum_{j=1}^{m}\sum_{i=1}^{n_j}\left[y_{ij} - f\left(x_{ij}, \theta_j\right)\right]^2 \frac{exp\left(\varphi_0 + \varphi_1\left(\frac{1}{TP_{in(ij)}}\right)\right)}{2}\right) \\
&\quad \times \prod_{j=1}^{m}\left(\frac{1}{2\pi\sqrt{|\Sigma_{\theta j}|}}\right) exp\left(-\frac{1}{2}\sum_{j=1}^{m}(\theta_j - \theta)^T \Sigma_{\theta j}^{-1} (\theta_j - \theta)\right) \\
&\quad \times \frac{1}{2\pi\sqrt{|\Sigma_\mu|}} exp\left(-\frac{1}{2}(\theta - \mu)^T \Sigma_\mu^{-1} (\theta - \mu)\right) \times \prod_{j=1}^{m\times\kappa} \frac{\beta_j^{\alpha j}}{\Gamma(\alpha_j)} \left(\sigma_j^2\right)^{-\alpha_j - 1} exp\left(-\frac{\beta_j}{\sigma_j^2}\right) \\
&\quad \times \frac{1}{2\pi\sqrt{|\Sigma_0|}} exp\left(-\frac{1}{2}(\mu - \mu_0)^T \Sigma_0^{-1} (\mu - \mu_0)\right) \times \frac{\beta_0^{\alpha_0}}{\Gamma(\alpha_0)} (\sigma^2)^{-\alpha_0 - 1} exp\left(-\frac{\beta_0}{\sigma^2}\right) \\
&\quad \times \frac{1}{2\pi\sqrt{|\Sigma_\varphi|}} exp\left(-\frac{1}{2}\left(\varphi - \varphi_\mu\right)^T \Sigma_\varphi^{-1} \left(\varphi - \varphi_\mu\right)\right)
\end{aligned}$$

where φ = vector of parameters $[\varphi_0, \varphi_1]$; φ_μ = vector of hyperparameters [0, 0]; and $\Sigma_\varphi = \begin{bmatrix} 10000 & 0 \\ 0 & 10000 \end{bmatrix}$.

The posterior of the hierarchical model with multivariate normal parameter prior is:

$$\begin{aligned}
&\pi\left(\theta', \theta, \Sigma_\theta, \mu, \tau^2 | x, y\right) = L\left(y|x, \theta', \tau^2\right) L\left(\theta' | \theta, \Sigma_\theta\right) L(\theta|\mu) \pi\left(\Sigma_\theta, \mu, \tau^2\right) \\
&= \left(\frac{1}{2\pi\tau^2}\right)^{\frac{N}{2}} exp\left(-\frac{1}{2\tau^2}\sum_{j=1}^{m}\sum_{i=1}^{n_j}\left[y_{ij} - f\left(x_{ij}, \theta_j\right)\right]^2\right) \\
&\quad \times \left(\frac{1}{\sqrt{2\pi|\Sigma_\theta|}}\right)^{\frac{m}{2}} exp\left(-\frac{1}{2}\sum_{j=1}^{m}(\theta_j - \theta)^T \Sigma_\theta^{-1} (\theta_j - \theta)\right) \\
&\quad \times \frac{1}{\sqrt{2\pi|\Sigma_\mu|}} exp\left(-\frac{1}{2}(\theta - \mu_0)^T \Sigma_\mu^{-1} (\theta - \mu_0)\right) \\
&\quad \times \frac{|R|^{\frac{\nu}{2}}}{2^{\frac{\nu\kappa}{2}} \Gamma_\kappa\left(\frac{\nu}{2}\right)} |\Sigma_\theta|^{-\frac{\nu+\kappa+1}{2}} exp\left(-\frac{1}{2} tr\left(R\Sigma_\theta^{-1}\right)\right) \\
&\quad \times \frac{\beta^\alpha}{\Gamma(\alpha)} \left(\tau^2\right)^{-\alpha - 1} exp\left(-\frac{\beta}{\tau^2}\right)
\end{aligned}$$

where $\nu > \kappa - 1$ the degrees of freedom set equal to 2, representing lack of confidence on the existing information.

Appendix C. Analytical solution for the mass-balance model forced with sinusoidal loading

The phosphorus mass balance for a finite time period can be expressed as:

$$V\frac{dTP}{dt} = W_{loading(t)} - Q \cdot TP - k \cdot V \cdot TP - \frac{v}{H} \cdot TP$$

which after simple mathematical manipulations leads to the following equation:

$$\frac{dTP}{dt} + \lambda \cdot TP = \frac{W_{loading(t)}}{V}.$$

Based on this equation and if we set $W_{loading(t)} = W_{avg} + W_{amplitude} \sin(\omega t - \theta)$, TP is equal to:

$$TP = e^{-\lambda t}\left[C_o + \int_o^t \underbrace{\frac{W_{avg} + W_{amplitude}\sin(\omega t - \theta)}{V} e^{\lambda t} dt}_{①.}\right]$$

The selected term ① can be decomposed into two terms:

$$\underbrace{\int_o^t \frac{W_{avg}}{V} e^{\lambda t} dt}_{②} + \underbrace{\int_o^t \frac{W_{amplitude}\sin(\omega t - \theta)}{V} e^{\lambda t} dt}_{③.}$$

The term ② is equal:

$$\int_o^t \frac{W_{avg}}{V} e^{\lambda t} dt = \frac{Wavg}{\lambda V} e^{\lambda t}.$$

The term ③ is:

$$\frac{W_{amplitude}}{V} \underbrace{\int_o^t \sin(\omega t - \theta)\ e^{\lambda t} dt}_{④}$$

and as shown in Box (1), the term ④ is equal:

$$\int_o^t sin(\omega t - \theta)\, e^{\lambda t} dt = \frac{\sin(\omega t - \theta - \varphi(\omega))\ e^{\lambda t}}{\sqrt{\lambda^2 + \omega^2}}.$$

Thus, the differential equation becomes:

$$\begin{aligned}
TP &= e^{-\lambda t}\left[C_o + \frac{W_{avg}}{\lambda V} e^{\lambda t} + \frac{W_{amplitude}}{V\sqrt{\lambda^2 + \omega^2}} \sin(\omega t - \theta - \varphi(\omega))\ e^{\lambda t}\right] \\
TP &= C_o\, e^{-\lambda t} + \frac{W_{avg}}{\lambda V} + \frac{W_{amplitude}}{V\sqrt{\lambda^2 + \omega^2}} \sin(\omega t - \theta - \varphi(\omega)) \\
&\quad if\ t \to 0 \\
TP = 0 &= TP_o + \frac{W_{avg}}{\lambda V} + \frac{W_{amplitude}}{V\sqrt{\lambda^2 + \omega^2}} \sin(-\theta - \varphi(\omega)) \\
TP_{o=} &- \frac{W_{avg}}{\lambda V} - \frac{W_{amplitude}}{V\sqrt{\lambda^2 + \omega^2}} \sin(-\theta - \varphi(\omega)).
\end{aligned}$$

The analytical solution of the differential equation becomes:

$$\begin{aligned}
TP &= \left[-\frac{W_{avg}}{\lambda V} - \frac{W_{amplitude}}{V\sqrt{\lambda^2 + \omega^2}} \sin(-\theta - \varphi(\omega))\right] e^{-\lambda t} + \frac{W_{avg}}{\lambda V} \\
&\quad + \frac{W_{amplitude}}{V\sqrt{\lambda^2 + \omega^2}} \sin(\omega t - \theta - \varphi(\omega)) \\
TP &= \frac{W_{avg}}{\lambda V}\left(1 - e^{-\lambda t}\right) + \frac{W_{amplitude}}{V\sqrt{\lambda^2 + \omega^2}} \sin(\omega t - \theta - \varphi(\omega)) \\
&\quad - \frac{W_{amplitude}}{V\sqrt{\lambda^2 + \omega^2}} \sin(-\theta - \varphi(\omega))\, e^{-\lambda t} \\
\varphi(\omega) &= \alpha rc\tan\left(\frac{\omega}{\lambda}\right)
\end{aligned}$$

if $t \to +\infty$ the final solution is:

$$TP = \frac{W_{avg}}{\lambda V} + \frac{W_{amplitude}}{V\sqrt{\lambda^2 + \omega^2}} \sin(\omega t - \theta - \varphi(\omega)).$$

Box 1

$$\int_o^t \sin(\omega t-\theta)e^{\lambda t}dt = \quad \text{(Integrated by parts rule)}$$

$$\frac{\sin(\omega t-\theta)e^{\lambda t}}{\lambda} - \frac{\omega}{\lambda}\int \cos(\omega t-\theta)e^{\lambda t}dt =$$

$$\frac{\sin(\omega t-\theta)e^{\lambda t}}{\lambda} - \frac{\omega}{\lambda^2}\cos(\omega t-\theta)e^{\lambda t} - \frac{\omega^2}{\lambda^2}\int \sin(\omega t-\theta)e^{\lambda t}dt =$$

$$\left(1+\frac{\omega^2}{\lambda^2}\right)\int_o^t \sin(\omega t-\theta)e^{\lambda t}dt = \frac{\sin(\omega t-\theta)\ e^{\lambda t}}{\lambda} - \frac{\omega}{\lambda^2}\cos(\omega t-\theta)e^{\lambda t} =$$

$$\left(\frac{\lambda^2+\omega^2}{\lambda^2}\right)\int_o^t \sin(\omega t-\theta)e^{\lambda t}dt = \frac{[\lambda\sin(\omega t-\theta)-\omega\cos(\omega t-\theta)]\ e^{\lambda t_*}}{\lambda^2} =$$

$$\frac{\sqrt{\lambda^2+\omega^2}\sin(\omega t-\theta-\varphi(\omega))e^{\lambda t}}{\lambda^2} \text{ with } \varphi = \alpha rc\tan\left(\frac{\omega}{\lambda}\right)$$

$$\left.\begin{array}{l} *\text{Because of the trigonometric identity}: \\ a\sin x + b\cos x = \sqrt{a^2+b^2}\sin(x+\varphi) \\ \varphi = \alpha rc\tan\left(\frac{b}{a}\right) + \left\{\begin{array}{ll} 0\ if & a \geq 0 \\ \pi\ if & a < 0 \end{array}\right\} \end{array}\right\}$$

Appendix D. Supplementary data

Supplementary data to this article can be found online at http://dx.doi.org/10.1016/j.ecoinf.2015.07.005.

References

Ahlgren, I., Frisk, T., Kampnielsen, L., 1988. Empirical and theoretical-models of phosphorus loading, retention and concentration vs lake trophic state. Hydrobiologia 170, 285–303. http://dx.doi.org/10.1007/BF00024910.

Borsuk, M.E., Higdon, D., Stow, C.A., Reckhow, K.H., 2001. A Bayesian hierarchical model to predict benthic oxygen demand from organic matter loading in estuaries and coastal zones. Ecol. Model. 143, 165–181. http://dx.doi.org/10.1016/S0304-3800(01)00328-3.

Brett, M.T., Benjamin, M.M., 2008. A review and reassessment of lake phosphorus retention and the nutrient loading concept. Freshw. Biol. 53, 194–211. http://dx.doi.org/10.1111/j.1365-2427.2007.01862.x.

Brooks, S.P., Gelman, A., 1998. General methods for monitoring convergence of iterative simulations. J. Comput. Graph. Stat. 7, 434–455. http://dx.doi.org/10.1080/10618600.1998.10474787.

Canfield, D., Bachmann, R., 1981. Prediction of total phosphorus concentrations, chlorophyll a, and secchi depths in natural and artificial lakes. Can. J. Fish. Aquat. Sci. 38, 414–423.

Chapra, S.C., Dolan, D.M., 2012. Great Lakes total phosphorus revisited: 2. Mass balance modeling. J. Great Lakes Res. 38, 741–754. http://dx.doi.org/10.1016/j.jglr.2012.10.002.

Chapra, S.C., Reckhow, K.H., 1979. Expressing the phosphorus loading concept in probabilistic terms. J. Fish. Res. Board Can. 36, 225–229. http://dx.doi.org/10.1139/f79-034.

Cheng, V., Arhonditsis, G.B., Brett, M.T., 2010. A revaluation of lake-phosphorus loading models using a Bayesian hierarchical framework. Ecol. Res. 25, 59–76. http://dx.doi.org/10.1007/s11284-009-0630-5.

Dillon, P.J., Molot, L.A., 1996. Long-term phosphorus budgets and an examination of a steady-state mass balance model for central Ontario Lakes. Water Res. 30, 2273–2280.

Dittrich, M., Chesnyuk, A., Gudimov, A., McCulloch, J., Quazi, S., Young, J., Winter, J., Stainsby, E., Arhonditsis, G., 2013. Phosphorus retention in a mesotrophic lake under transient loading conditions: insights from a sediment phosphorus binding form study. Water Res. 47, 1433–1447. http://dx.doi.org/10.1016/j.watres.2012.12.006.

Gelman, A., Hill, J., 2007. Data Analysis Using Regression and Multilevel/Hierarchical Models. 2nd ed. Cambridge University Press, New York.

Gilks, W.R., Roberts, G.O., Sahu, S.K., 1998. Adaptive Markov chain Monte Carlo through regeneration. J. Am. Stat. Assoc. 93, 1045–1054. http://dx.doi.org/10.2307/2669848.

Gudimov, A., O'Connor, E., Dittrich, M., Jarjanazi, H., Palmer, M.E., Stainsby, E., Winter, J.G., Young, J.D., Arhonditsis, G.B., 2012. Continuous Bayesian network for studying the causal links between phosphorus loading and plankton patterns in Lake Simcoe, Ontario, Canada. Environ. Sci. Technol. 46, 7283–7292. http://dx.doi.org/10.1021/es300983r.

Gudimov, A., Kim, D.-K., Young, J.D., Palmer, M.E., Dittrich, M., Winter, J.G., Stainsby, E., Arhonditsis, G.B., 2015. Examination of the role of dreissenids and macrophytes in the phosphorus dynamics of Lake Simcoe, Ontario, CanadaEcol. Inform. 26 pp. 36–53. http://dx.doi.org/10.1016/j.ecoinf.2014.11.007 (Part 3).

Hecky, R.E., Smith, R.E.H., Barton, D.R., Guildford, S.J., Taylor, W.D., Charlton, M.N., Howell, T., 2004. The nearshore phosphorus shunt: a consequence of ecosystem engineering by dreissenids in the Laurentian Great Lakes. Can. J. Fish. Aquat. Sci. 61, 1285–1293. http://dx.doi.org/10.1139/F04-065.

Higgins, J.M., Kim, B.R., 1981. Phosphorus retention models for Tennessee valley authority reservoirs. Water Resour. Res. 17 (3), 571–576. http://dx.doi.org/10.1029/WR017i003p00571.

Hiriart-Baer, V.P., Milne, J.E., Marvin, C.H., 2011. Temporal trends in phosphorus and lacustrine productivity in Lake Simcoe inferred from lake sediment. J. Great Lakes Res. 37, 764–771. http://dx.doi.org/10.1016/j.jglr.2011.08.014.

Jensen, J.P., Pedersen, A.R., Jeppesen, E., Søndergaard, M., 2006. An empirical model describing the seasonal dynamics of phosphorus in 16 shallow eutrophic lakes after external loading reduction. Limnol. Oceanogr. 51, 791–800. http://dx.doi.org/10.4319/lo.2006.51.1_part_2.0791.

Judge, G.G., Griffiths, W.E., Carter Hill, R., Lütkepohl, H., Lee, T.-C., 1985. The Theory and Practice of Econometrics. 2nd ed. Wiley, New York.

Kim, D.-K., Zhang, W., Rao, Y.R., Watson, S., Mugalingam, S., Labencki, T., Dittrich, M., Morley, A., Arhonditsis, G.B., 2013. Improving the representation of internal nutrient recycling with phosphorus mass balance models: a case study in the Bay of Quinte, Ontario, Canada. Ecol. Model. 256, 53–68. http://dx.doi.org/10.1016/j.ecolmodel.2013.02.017.

Larsen, D.P., Mercier, H.T., 1976. Phosphorus retention capacity of lakes. J. Fish. Res. Board Can. 33, 1742–1750.

Lunn, D.J., Thomas, A., Best, N., Spiegelhalter, D., 2000. WinBUGS — a Bayesian modelling framework: concepts, structure, and extensibility. Stat. Comput. 10, 325–337. http://dx.doi.org/10.1023/A:1008929526011.

Malmaeus, J.M., Håkanson, L., 2004. Development of a lake eutrophication model. Ecol. Model. 171, 35–63. http://dx.doi.org/10.1016/S0304-3800(03)00297-7.

Malve, O., Qian, S.S., 2006. Estimating nutrients and chlorophyll a relationships in Finnish Lakes. Environ. Sci. Technol. 40, 7848–7853.

Nürnberg, G.K., LaZerte, B.D., 2004. Modeling the effect of development on internal phosphorus load in nutrient-poor lakes. Water Resour. Res. 40, W01105. http://dx.doi.org/10.1029/2003WR002410.

Prairie, Y.T., Marshall, C.T., 1995. On the use of structured time-series to detect and test hypotheses about within-lakes relationships. Can. J. Fish. Aquat. Sci. 52, 799–803. http://dx.doi.org/10.1139/f95-079.

Reckhow, K.H., 1993. A random coefficient model for chlorophyll–nutrient relationships in lakes. Ecol. Model. 70, 35–50. http://dx.doi.org/10.1016/0304-3800(93)90071-Y.

Reckhow, K.H., Chapra, S.C., 1983. Confirmation of water quality models. Ecol. Model. 20, 113–133.

Scheffer, M., 2004. Ecology of Shallow Lakes. Springer Science & Business Media.

Schindler, D., Fee, E., Ruszczynski, T., 1978. Phosphorus input and its consequences for phytoplankton standing crop and production in experimental lakes area and in similar lakes. J. Fish. Res. Board Can. 35, 190–196.

Shimoda, Y., Azim, M.E., Perhar, G., Ramin, M., Kenney, M.A., Sadraddini, S., Gudimov, A., Arhonditsis, G.B., 2011. Our current understanding of lake ecosystem response to climate change: what have we really learned from the north temperate deep lakes? J. Great Lakes Res. 37, 173–193. http://dx.doi.org/10.1016/j.jglr.2010.10.004.

Søndergaard, M., Jensen, J.P., Jeppesen, E., 2003. Role of sediment and internal loading of phosphorus in shallow lakes. Hydrobiologia 506–509, 135–145. http://dx.doi.org/10.1023/B:HYDR.0000008611.12704.dd.

Spiegelhalter, D.J., Best, N.G., Carlin, B.P., Van Der Linde, A., 2002. Bayesian measures of model complexity and fit. J. R. Stat. Soc. Ser. B Stat. Methodol. 64, 583–639. http://dx.doi.org/10.1111/1467-9868.00353.

Stow, C.A., Dyble, J., Kashian, D.R., Johengen, T.H., Winslow, K.P., Peacor, S.D., Francoeur, S.N., Burtner, A.M., Palladino, D., Morehead, N., Gossiaux, D., Cha, Y., Qian, S.S., Miller, D., 2014. Phosphorus targets and eutrophication objectives in Saginaw Bay: a 35 year assessment. J. Great Lakes Res. 40 (Supplement 1), 4–10. http://dx.doi.org/10.1016/j.jglr.2013.10.003 (The Continuing Effects of Multiple Stressors in Saginaw Bay).

Swamy, P.A.V.B., 1971. Statistical Inference in Random Coefficient Regression Models. Springer, Berlin Heidelberg.

Uttormark, P.D., Hutchins, M.L., 1978. Input–output Models as Decisions Criteria for Lake Restoration, Technical Report. Unites States Department of the Interior, Office of Water Research and Technology.

Vollenweider, R.A., 1969. Möglichkeiten und grenzen elementarer modelle der stoffbilanz von seen. Arch. Hydrobiol. 66, 1–36.

Vollenweider, R.A., 1975. Input output models with special reference to the phosphorus loading concept in limnology. Schweiz. Z. Fuer Hydrol. 37, 53–84. http://dx.doi.org/10.1007/BF02505178.

Vollenweider, R.A., 1976. Advances in defining critical loading levels for phosphorus in lake eutrophication. Mem. DellIstituto Ital. Idrobiol. Dott Marco Marchi 33, 53–83.

Walker, W.W.J., 1977. Some Analytical Methods Applied to Lake Water Quality Problems. Harvard University, Cambridge, MA.

Young, J.D., Winter, J.G., Molot, L., 2011. A re-evaluation of the empirical relationships connecting dissolved oxygen and phosphorus loading after dreissenid mussel invasion in Lake Simcoe. J. Great Lakes Res. 37 (Supplement 3), 7–14. http://dx.doi.org/10.1016/j.jglr.2010.12.008.

Zhang, W., Arhonditsis, G.B., 2009. A Bayesian hierarchical framework for calibrating aquatic biogeochemical models. Ecol. Model. 220, 2142–2161. http://dx.doi.org/10.1016/j.ecolmodel.2009.05.023.

INTEGRATING HIERARCHICAL BAYES WITH PHOSPHORUS LOADING MODELLING

(Electronic Supplementary Material)

Yuko Shimoda and George B. Arhonditsis*

Ecological Modelling Laboratory

Department of Physical & Environmental Sciences, University of Toronto,

Toronto, Ontario, Canada, M1C 1A4

* Corresponding author

e-mail: georgea@utsc.utoronto.ca, Tel.: +1 416 208 4858; Fax: +1 416 287 7279.

DESCRIPTION OF LAKE SIMCOE

Lake Simcoe is the largest lake in Southern Ontario (after the Great Lakes) with a surface area of 722 km^2, watershed area of 2,899 km^2, and a maximum and mean depth of 42 m and 14.2 m, respectively. Lake Simcoe experienced severe eutrophication problems as a result of the agricultural practices and increasing urbanization in its catchment since 1930s (North, 2013). The eutrophication problems became particularly severe in the 1970s with excessive algal and macrophyte growth, and more recently, hypolimnetic hypoxia has been occasionally manifested at the end of summer stratification period (Eimers *et al.*, 2005). Despite continuous efforts to reduce *P* loading (Winter *et al.*, 2002), only subtle water quality improvements have been experienced and the ambient *TP* concentrations in Lake Simcoe have not declined accordingly (Young *et al.*, 2010).

Lake Simcoe is generally divided into three morphologically distinct regions: (*i*) Kempenfelt Bay, a narrow and the deep embayment with surface area of 34 km^2 and mean depth of 20 m, is located near the city of Barrie at the south west corner of the lake. The urbanization activities associated with the rapid population growth of the City of Barrie are the main vector of P loading into the bay, resulting in fairly high *TP* concentration in the water column, e.g., 14.0 ±2.7 μg *TP* L^{-1} (Dittrich *et al.*, 2013). Oxygen depletion in the hypolimnion also occurs at the end of the summer in Kempenfelt Bay, which may contribute to high P release into the water column (Dittrich *et al.*, 2013). (*ii*) The Cook's Bay with a mean depth of 13 m, maximum depth of 15 m and a surface area of 45 km^2. This embayment is located at the southern end of the lake near Holland March, where the dominant use of the watershed is agriculture (43% of total watershed area). Cook's Bay receives approximately twice the external P loading that Kempenfelt Bay receives, resulting in distinctly higher ambient *TP* levels (18.4 ±7.7 μg *TP* L^{-1}). The shallow morphometry of the bay provides a desirable habitat for macrophytes that significantly influence the P dynamics through significant *P* uptake from the sediments and *P* release via the decomposition of the dead plant tissues (Bini *et al.*, 2010). The largest, main basin has a mean depth of 14 m, maximum depth of 33 m and surface area of 643 m^2. The catchment of this basin experienced gradual deforestation, which has been the one of the main driver of the *TP* loading variability. Because of its shallow morphometry, a large portion of the eastern area of the bay is located

within the euphotic and well-mixed zone, and thus the elevated benthic photosynthesis and access of the dreissenids to sestonic algae create favorable conditions for biodeposition and nutrient recycling (Ozersky *et al.*, 2013). More than 50% of the total dreissenid biomass (≈12 tonnes of shell-free dry mass) is found in Kempenfelt Bay and the main basin, areas with depth up to 8 m (see Fig. 1 in Schwalb *et al.*, 2013). Dreissenid mussels can take up considerable amount of particulate matter from the water column; however, the net P removal is significantly lower due to the high P release rate as faces, pseudofeces or other metabolic excreta (Gudimov *et al.*, 2015). The internal nutrient regeneration mechanisms through dreissenid mussel activity, proliferation of macrophytes (Gudimov et al., 2015), and the interplay between water column and sediments (Dittrich et al., 2013, Gudimov et al., 2015) have been hypothesized as a key regulatory factor that determines the spatially and temporally variability of phosphorous dynamics in Lake Simcoe.

Table S1: Lake characteristics and observed TP_{lake} (µg L^{-1}) concentrations of the eight terminal nodes identified by *CART* analysis (Cheng et al., 2010).

Class	Number of sample	Depth (m)	Surface area (km^2)	Residence time (yr)	Median TP_{lake} (µg L^{-1})	TP range* (µg L^{-1})
I	30	$z \leq 1.65$			160.0	989.5
II	34	$1.65 < z \leq 10.3$	$A \leq 1.47$		20.8	173.9
III	35	$1.65 < z \leq 10.3$	$1.47 < A \leq 20.3$	$\tau_w \leq 0.17$	45.0	261.6
IV	60	$1.65 < z \leq 10.3$	$1.47 < A \leq 20.3$	$\tau_w > 0.17$	70.5	491.0
V	40	$1.65 < z \leq 10.3$	$A > 20.3$		33.5	162.4
VI	85	$z > 10.3$		$\tau_w \leq 9.8$	14.5	113.2
VII	7	$z > 10.3$		$9.8 < \tau_w \leq 17.8$	73.9	232.0
VIII	14	$z > 10.3$		$\tau_w > 17.8$	8.8	33.0

* The values represent the difference between the 95th and 5th percentiles.

Table S2: Posterior statistics of sedimentation rates between two scenarios of high (present average values increased by 10 µg *TP* L^{-1}) and low (present levels) *TP* concentrations in the Eastern Basin of Lake Simcoe.

	Low		High	
	Mean	SD	Mean	SD
Cook's Bay	1.077	0.437	1.065	0.444
Kempenfelt Bay	0.851	0.212	0.841	0.208
Eastern Basin	0.753	0.102	0.317	0.071
Main Basin	0.636	0.091	0.690	0.106
Atherley Narrows	0.659	0.329	0.651	0.313

FIGURES LEGENDS

Figure S1: Scatter plots of the pooling factor λ for the two adjustable constant parameters k (a, b) and x (c, d) from the Multivariate Normal (left panel) and Classical Hierarchical (right panel) models.

Figure S2: Annual *TP* fluxes (mg m^{-2} yr^{-1}) of each segment under two scenarios of high (present average values increased by 10 µg *TP* L^{-1}) and low (present levels) *TP* concentrations in Eastern Basin of Lake Simcoe. Values provided in bracket represent the scenario of high *TP* concentrations.

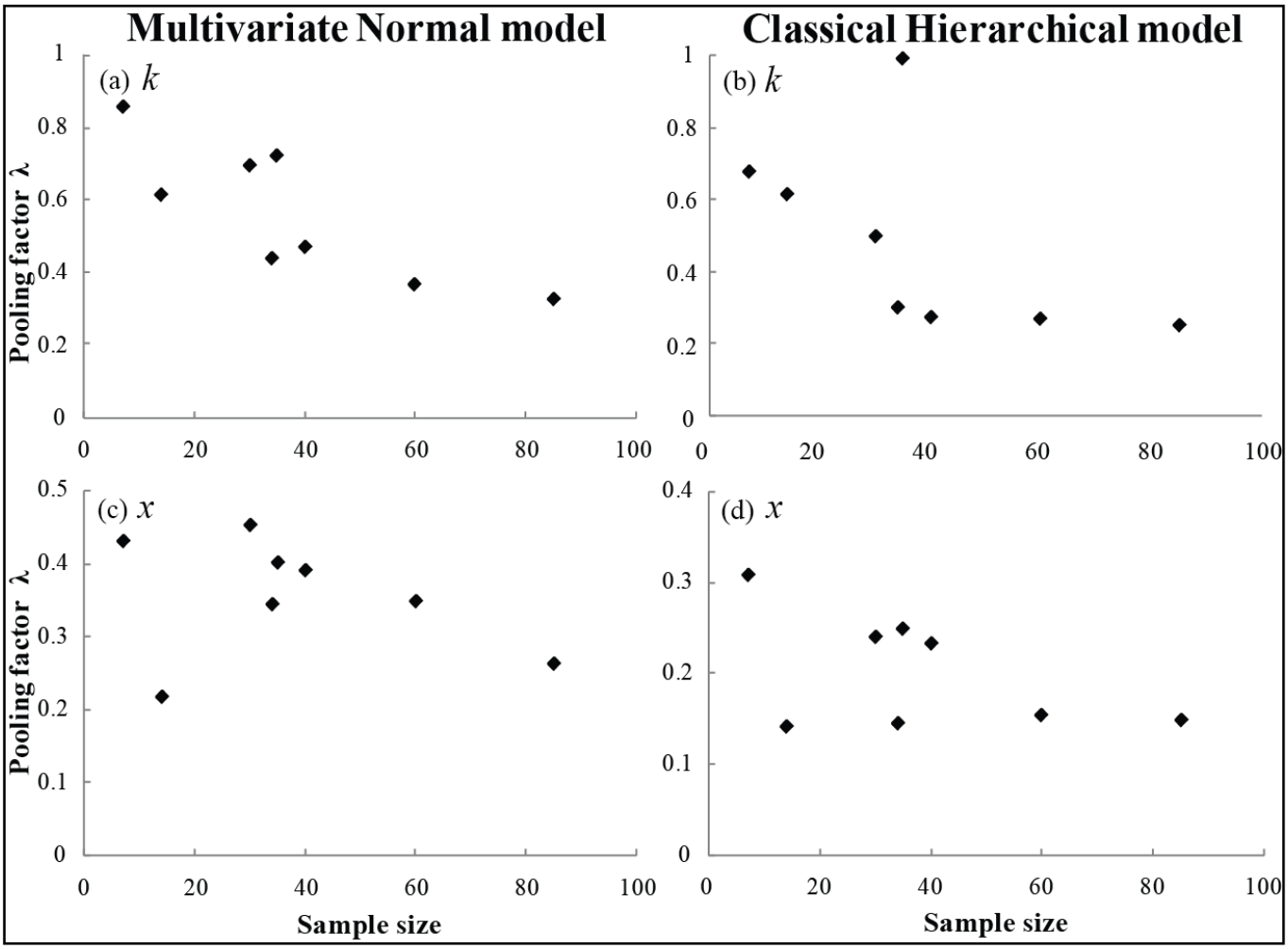
Multivariate Normal model
Classical Hierarchical model
(a) k
(b) k
(c) x
(d) x
Pooling factor λ
Pooling factor λ
Sample size
Sample size

Figure S1

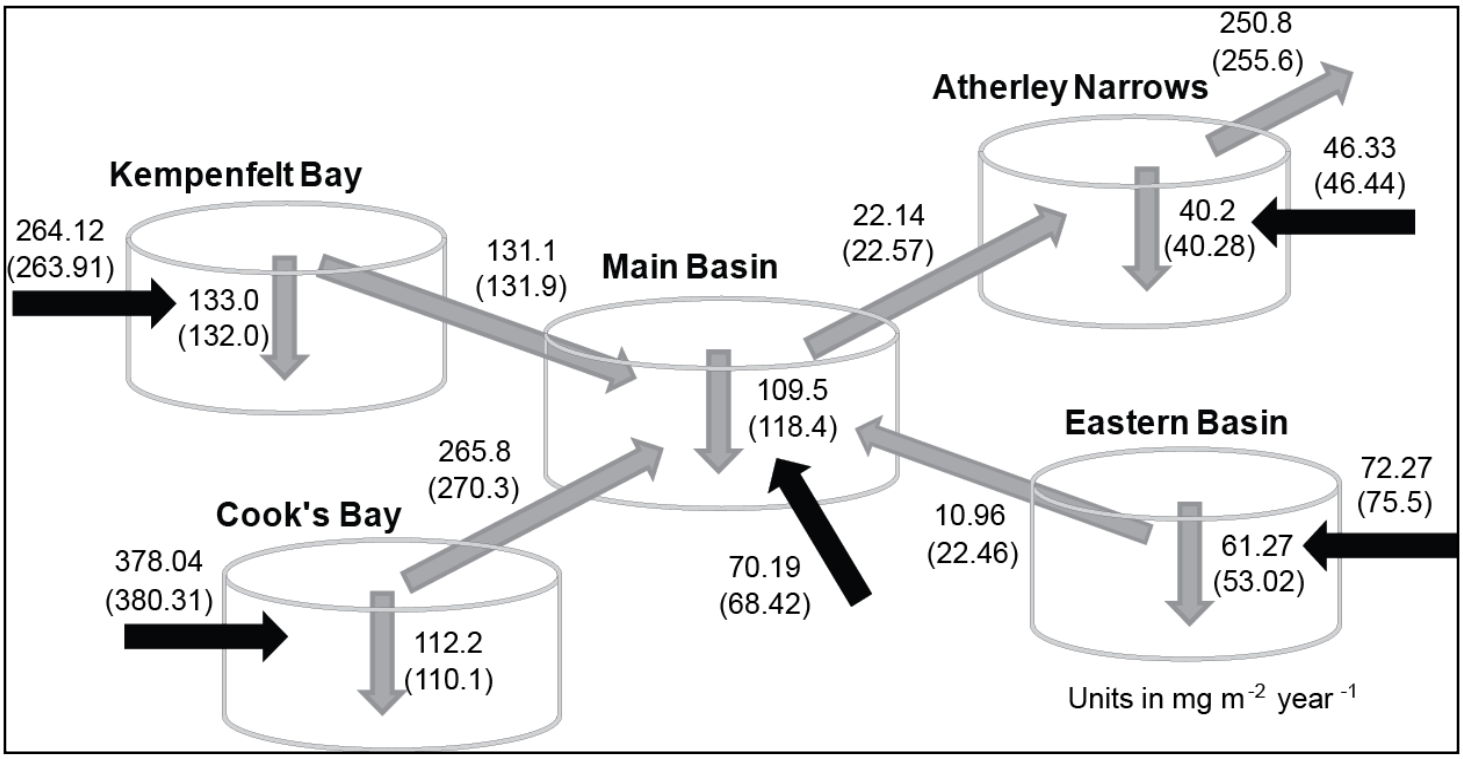
Kempenfelt Bay
Atherley Narrows
Main Basin
Eastern Basin
Cook's Bay
264.12
(263.91)
133.0
(132.0)
131.1
(131.9)
22.14
(22.57)
250.8
(255.6)
46.33
(46.44)
40.2
(40.28)
109.5
(118.4)
265.8
(270.3)
378.04
(380.31)
112.2
(110.1)
70.19
(68.42)
10.96
(22.46)
72.27
(75.5)
61.27
(53.02)
Units in mg m-2 year -1

Figure S2

Bayesian reassessment of the lake phosphorus retention & loading concept in limnology

The WinBUGS codes associated with the lake phosphorus loading models are as follows:

Model 1 (Classical) :

```
model {

for (i in 1:N) {
TPlakem1[i]<-log(TPinput1[i]/(1+k4l[1]*mu1[i]) )
mu1[i]<-pow(tw1[i], x4l[1])
TPlake1[i]~dnorm(TPlakem1[i],tau)
LPredTPlake1[i]~dnorm(TPlakem1[i],tau)
PredTPlake1[i]<-exp(LPredTPlake1[i])}
for (i in 1:M) {
TPlakem2[i]<-log(TPinput2[i]/(1+k4l[2]*mu2[i]) )
mu2[i]<-pow(tw2[i], x4l[2])
TPlake2[i]~dnorm(TPlakem2[i],tau)
LPredTPlake2[i]~dnorm(TPlakem2[i],tau)
PredTPlake2[i]<-exp(LPredTPlake2[i])}
for (i in 1:2) {
k4l[i]~dnorm(k4,kltau[i])I(0,)
kltau[i]~dgamma(0.001,0.001)
klsigma[i]<-sqrt(1/kltau[i])
x4l[i]~dnorm(x4, xltau[i])I(0,)
xltau[i]~dgamma(0.001,0.001)
xlsigma[i]<-sqrt(1/xltau[i])}
k4~dnorm(kmu,ktau)I(0,)
kmu~dnorm(0,0.0001)I(0,)
ktau~dgamma(0.001,0.001)
ksigma<-sqrt(1/ktau)
x4~dnorm(xmu,xtau)I(0,)
xmu~dnorm(0,0.0001)I(0,)
xtau~dgamma(0.001,0.001)
xsigma<-sqrt(1/xtau)
sigma<-sqrt(1/tau)
tau~dunif(0.01,100)
}
```

Inference Data

list(N=199,
tw1=c(***paste tw1.dat here***),
TPinput1=c(***paste TPinput1.dat here***),
TPlake1=c(***paste TPlake1.dat here***),
M=106,
tw2=c(***paste tw2.dat here***),
TPlake2=c(***paste TPlake2.dat here***))

Initial values 1

list(k4=1, x4=1, kmu=1, xmu=1, k4l=c(1,1), x4l=c(1,1), tau =1, ktau=1, xtau=1,kltau=c(1,1), xltau=c(1,1),
LPredTPlake1=c(***paste LPredTPlake1.dat here***),

LPredTPlake2=c(***paste LPredTPlake2.dat here***))

Initial values 2
list(k4=0.1, x4=0.1, kmu=0.1, xmu=0.1, k4l=c(0.1,0.1), x4l=c(0.1,0.1), tau =0.1, ktau=0.1,
xtau=0.1,kltau=c(0.1,0.1), xltau=c(0.1,0.1),
LPredTPlake1=c(***paste LPredTPlake1.dat here***),
LPredTPlake2=c(***paste LPredTPlake2.dat here***))

Initial values 3
list(k4=2, x4=2, kmu=2, xmu=2, k4l=c(2,2), x4l=c(2,2), tau =2, ktau=2, xtau=2,kltau=c(2,2), xltau=c(2,2),
LPredTPlake1=c(***paste LPredTPlake1.dat here***),
LPredTPlake2=c(***paste LPredTPlake2.dat here***))

Model 2 (Informative Global Prior)

```
model {

for (i in 1:N) {
TPlakem1[i]<-log(TPinput1[i]/(1+k4l[1]*mu1[i]) )
mu1[i]<-pow(tw1[i], x4l[1])
TPlake1[i]~dnorm(TPlakem1[i],tau)
LPredTPlake1[i]~dnorm(TPlakem1[i],tau)
PredTPlake1[i]<-exp(LPredTPlake1[i])}
for (i in 1:M) {
TPlakem2[i]<-log(TPinput2[i]/(1+k4l[2]*mu2[i]) )
mu2[i]<-pow(tw2[i], x4l[2])
TPlake2[i]~dnorm(TPlakem2[i],tau)
LPredTPlake2[i]~dnorm(TPlakem2[i],tau)
PredTPlake2[i]<-exp(LPredTPlake2[i])}
for (i in 1:2) {
k4l[i]~dnorm(k4,kltau[i])I(0,)
kltau[i]~dgamma(0.001,0.001)
klsigma[i]<-sqrt(1/kltau[i])
x4l[i]~dnorm(x4, xltau[i])I(0,)
xltau[i]~dgamma(0.001,0.001)
xlsigma[i]<-sqrt(1/xltau[i])}
k4~dnorm(kmu,ktau)I(0,)
kmu~dnorm(1.12,156.25)I(0,)
ktau~dgamma(0.001,0.001)
ksigma<-sqrt(1/ktau)
x4~dnorm(xmu,xtau)I(0,)
xmu~dnorm(0.47,625)I(0,)
xtau~dgamma(0.001,0.001)
xsigma<-sqrt(1/xtau)
sigma<-sqrt(1/tau)
tau~dunif(0.01,100)
}
```

Inference Data

list(N=199,
tw1=c(***paste tw1.dat here***),
TPinput1=c(***paste TPinput1.dat here***),
TPlake1=c(***paste TPlake1.dat here***),
M=106,
tw2=c(***paste tw2.dat here***),
TPinput2=c(***paste TPinput2.dat here***),
TPlake2=c(***paste TPlake2.dat here***))

Initial values 1
list(k4=1, x4=1, kmu=1, xmu=1, k4l=c(1,1), x4l=c(1,1), tau =1, ktau=1, xtau=1,kltau=c(1,1), xltau=c(1,1),
LPredTPlake1=c(***paste LPredTPlake1.dat here***),
LPredTPlake2=c(***paste LPredTPlake2.dat here***))

Initial values 2
list(k4=0.1, x4=0.1, kmu=0.1, xmu=0.1, k4l=c(0.1,0.1), x4l=c(0.1,0.1), tau =0.1, ktau=0.1,
xtau=0.1,kltau=c(0.1,0.1), xltau=c(0.1,0.1),
LPredTPlake1=c(***paste LPredTPlake1.dat here***),
LPredTPlake2=c(***paste LPredTPlake2.dat here***))

Initial values 3
list(k4=2, x4=2, kmu=2, xmu=2, k4l=c(2,2), x4l=c(2,2), tau =2, ktau=2, xtau=2,kltau=c(2,2), xltau=c(2,2),
LPredTPlake1=c(***paste LPredTPlake1.dat here***),
LPredTPlake2=c(***paste LPredTPlake2.dat here***))

Model 3 (Alternative Model Error)

model {

for (i in 1:N) {
TPlakem1[i]<-log(TPinput1[i]/(1+k4l[1]*mu1[i]))
mu1[i]<-pow(tw1[i], x4l[1])
TPlake1[i]~dnorm(TPlakem1[i],tau1[i])
LPredTPlake1[i]~dnorm(TPlakem1[i],tau1[i])
log(tau1[i])<-theta_error+phi*(1/TPinput1[i])
sigma1[i]<-sqrt(1/tau1[i])
PredTPlake1[i]<-exp(LPredTPlake1[i])}
for (i in 1:M) {
TPlakem2[i]<-log(TPinput2[i]/(1+k4l[2]*mu2[i]))
mu2[i]<-pow(tw2[i], x4l[2])
TPlake2[i]~dnorm(TPlakem2[i],tau2[i])
LPredTPlake2[i]~dnorm(TPlakem2[i],tau2[i])
log(tau2[i])<-theta_error+phi*(1/TPinput2[i])
sigma2[i]<-sqrt(1/tau2[i])
PredTPlake2[i]<-exp(LPredTPlake2[i])}
for (i in 1:2) {
k4l[i]~dnorm(k4,kltau[i])I(0,)
kltau[i]~dgamma(0.001,0.001)
klsigma[i]<-sqrt(1/kltau[i])
x4l[i]~dnorm(x4, xltau[i])I(0,)

xltau[i]~dgamma(0.001,0.001)
xlsigma[i]<-sqrt(1/xltau[i])}
k4~dnorm(kmu,ktau)I(0,)
kmu~dnorm(0,0.0001)I(0,)
ktau~dgamma(0.001,0.001)
ksigma<-sqrt(1/ktau)
x4~dnorm(xmu,xtau)I(0,)
xmu~dnorm(0,0.0001)I(0,)
xtau~dgamma(0.001,0.001)
xsigma<-sqrt(1/xtau)
theta_error~dnorm(0,0.0001)
phi~dnorm(0,0.0001)
}

Inference Data
list(N=199,
tw1=c(***paste tw1.dat here***),
TPinput1=c(***paste TPinput1.dat here***),
TPlake1=c(***paste TPlake1.dat here***),
M=106,
tw2=c(***paste tw2.dat here***),
TPinput2=c(***paste TPinput2.dat here***),
TPlake2=c(***paste TPlake2.dat here***))

Initial values 1
list(k4=1, x4=1, kmu=1, xmu=1, k4l=c(1,1), x4l=c(1,1), phi =0.5, theta_error=0.2, ktau=1,
xtau=1,kltau=c(1,1), xltau=c(1,1),
LPredTPlake1=c(***paste LPredTPlake1.dat here***),
LPredTPlake2=c(***paste LPredTPlake2.dat here***))

Initial values 2
list(k4=0.1, x4=0.1, kmu=0.1, xmu=0.1, k4l=c(0.1,0.1), x4l=c(0.1,0.1), phi =0.5, theta_error=0.2, ktau=0.1,
xtau=0.1,kltau=c(0.1,0.1), xltau=c(0.1,0.1),
LPredTPlake1=c(***paste LPredTPlake1.dat here***),
LPredTPlake2=c(***paste LPredTPlake2.dat here***))

Initial values 3
list(k4=2, x4=2, kmu=2, xmu=2, k4l=c(2,2), x4l=c(2,2), phi =0.5, theta_error=0.2, ktau=2,
xtau=2,kltau=c(2,2), xltau=c(2,2),
LPredTPlake1=c(***paste LPredTPlake1.dat here***),
LPredTPlake2=c(***paste LPredTPlake2.dat here***))

Model 4 (Multivariate Normal)

model {

for (i in 1:N) {
TPlakem1[i]<-log(TPinput1[i]/(1+theta[1,1]*mu1[i]))
mu1[i]<-pow(tw1[i], theta[1,2])
TPlake1[i]~dnorm(TPlakem1[i],mtau)

```
LPredTPlake1[i]~dnorm(TPlakem1[i],mtau)
PredTPlake1[i]<-exp(LPredTPlake1[i])}
for (i in 1:M) {
TPlakem2[i]<-log(TPinput2[i]/(1+theta[2,1]*mu2[i]) )
mu2[i]<-pow(tw2[i], theta[2,2])
TPlake2[i]~dnorm(TPlakem2[i],mtau)
LPredTPlake2[i]~dnorm(TPlakem2[i],mtau)
PredTPlake2[i]<-exp(LPredTPlake2[i])}
for (i in 1:2) {
theta[i, 1:2] ~ dmnorm(gmu[1:2], gtau[1:2, 1:2])I(Q[],)}
gmu[1:2] ~ dmnorm(mean[1:2], prec[1:2, 1:2])I(Q[],)
gtau[1:2, 1:2] ~ dwish(R[1:2, 1:2], 2)
sigma2[1:2, 1:2] <- inverse(gtau[1:2, 1:2])
for (i in 1:2) {sigma[i] <- sqrt(sigma2[i, i])}
msigma<-sqrt(1/mtau)
mtau~dunif(0.01,100)
}
```

Inference Data

```
list(mean = c(0, 0),Q=c(0,0),
                        R = structure(.Data = c(0.1, 0,
                                                0, 0.1), .Dim = c(2, 2)),
                      prec = structure(.Data = c(1.0E-6, 0,
                                                 0, 1.0E-6), .Dim = c(2, 2)),
N=199,
tw1=c(paste tw1.dat here),
TPinput1=c(paste TPinput1.dat here),
TPlake1=c(paste TPlake1.dat here),
M=106,
tw2=c(paste tw2.dat here),
TPinput2=c(paste TPinput2.dat here),
TPlake2=c(paste TPlake2.dat here))
```

Initial values 1

```
list(mtau =1, theta = structure(.Data = c(1.12, 0.47,
                                          1.12, 0.47),.Dim = c(2, 2)),
              gmu = c(1.12, 0.47),
              gtau = structure(.Data = c(0.1, 0,
                                         0, 0.1), .Dim = c(2, 2)),
LPredTPlake1=c(paste LPredTPlake1.dat here),
LPredTPlake2=c(paste LPredTPlake2.dat here))
```

Initial values 2

```
list(mtau =0.1, theta = structure(.Data = c(2, 0.5,
                                            2, 0.5),.Dim = c(2, 2)),
                gmu = c(2, 0.5),
                gtau = structure(.Data = c(0.1, 0,
                                           0, 0.1), .Dim = c(2, 2)),
LPredTPlake1=c(paste LPredTPlake1.dat here),
LPredTPlake2=c(paste LPredTPlake2.dat here))
```

Initial values 3

```
list(mtau =0.01, theta = structure(Data = c(1, 0.5,
                                            1, 0.5),.Dim = c(2, 2)),
                gmu = c(1, 0.5),
                gtau = structure(.Data = c(0.1, 0,
                                           0, 0.1), .Dim = c(2, 2)),
LPredTPlake1=c(paste LPredTPlake1.dat here),
LPredTPlake2=c(paste LPredTPlake2.dat here))
```

Model 5 (Multivariate Normal & Alternative Error)

```
model {

for (i in 1:N) {
TPlakem1[i]<-log(TPinput1[i]/(1+theta[1,1]*mu1[i]) )
mu1[i]<-pow(tw1[i], theta[1,2])
TPlake1[i]~dnorm(TPlakem1[i],mtau1[i])
LPredTPlake1[i]~dnorm(TPlakem1[i],mtau1[i])
log(mtau1[i])<-theta_error+phi*(1/TPinput1[i])
msigma1[i]<-sqrt(1/mtau1[i])
PredTPlake1[i]<-exp(LPredTPlake1[i])}
for (i in 1:M) {
TPlakem2[i]<-log(TPinput2[i]/(1+theta[2,1]*mu2[i]) )
mu2[i]<-pow(tw2[i], theta[2,2])
TPlake2[i]~dnorm(TPlakem2[i],mtau2[i])
LPredTPlake2[i]~dnorm(TPlakem2[i],mtau2[i])
log(mtau2[i])<-theta_error+phi*(1/TPinput2[i])
msigma2[i]<-sqrt(1/mtau2[i])
PredTPlake2[i]<-exp(LPredTPlake2[i])}
for (i in 1:2) {
theta[i, 1:2] ~ dmnorm(gmu[1:2], gtau[1:2, 1:2])I(Q[],)}
gmu[1:2] ~ dmnorm(mean[1:2], prec[1:2, 1:2])I(Q[],)
gtau[1:2, 1:2] ~ dwish(R[1:2, 1:2], 2)
sigma2[1:2, 1:2] <- inverse(gtau[1:2, 1:2])
for (i in 1:2) {sigma[i] <- sqrt(sigma2[i, i])}
theta_error~dnorm(0,0.0001)
phi~dnorm(0,0.0001)
}
```

Inference Data

```
list(mean = c(0, 0),Q=c(0,0),
                R = structure(.Data = c(0.1, 0,
                                        0, 0.1), .Dim = c(2, 2)),
                prec = structure(.Data = c(1.0E-6, 0,
                                           0, 1.0E-6), .Dim = c(2, 2)),
N=199,
tw1=c(paste tw1.dat here),
TPinput1=c(paste TPinput1.dat here),
TPlake1=c(paste TPlake1.dat here),
```

M=106,
tw2=c(***paste tw2.dat here***),
TPinput2=c(***paste TPinput2.dat here***),
TPlake2=c(***paste TPlake2.dat here***))

Initial values 1

```
list(phi =0.5, theta_error=0.2, theta = structure(.Data = c(1.12, 0.47,
                                                            1.12, 0.47),.Dim = c(2, 2)),
                                gmu = c(1.12, 0.47),
                                gtau = structure(.Data = c(0.1, 0,
                                                           0, 0.1), .Dim = c(2, 2)),
```

LPredTPlake1=c(***paste LPredTPlake1.dat here***),
LPredTPlake2=c(***paste LPredTPlake2.dat here***))

Initial values 2

```
list(phi =0.25, theta_error=0.4, theta = structure(.Data = c(2, 0.5,
                                                             2, 0.5),.Dim = c(2, 2)),
                                 gmu = c(2, 0.5),
                                 gtau = structure(.Data = c(0.1, 0,
                                                            0, 0.1), .Dim = c(2, 2)),
```

LPredTPlake1=c(***paste LPredTPlake1.dat here***),
LPredTPlake2=c(***paste LPredTPlake2.dat here***))

Initial values 3

```
list(phi =0.15, theta_error=0.1, theta = structure(.Data = c(1, 0.5,
                                                             1, 0.5),.Dim = c(2, 2)),
                                 gmu = c(1, 0.5),
                                 gtau = structure(.Data = c(0.1, 0,
                                                            0, 0.1), .Dim = c(2, 2)),
```

LPredTPlake1=c(***paste LPredTPlake1.dat here***),
LPredTPlake2=c(***paste LPredTPlake2.dat here***))

Continuously Stirred Tank Reactor Hierarchical Model with sinusoidal loading

```
model {

for (t in 1:L){
     for (i in 1:M) {
TPmodel_cbm[t,i]<- max(0.0001,Wmean_cb[t]/(lamda_cb[t,i]*volume_cb[t,i])
                       +(Wamp_cb[t]/(volume_cb[t,i]*sqrt(pow(lamda_cb[t,i],2)
                       +pow(omega,2))))*sin(omega*time[t,i]-theta_cb[t]-phi_cb[t,i]))

TPmodel_cb[t,i]<-log(TPmodel_cbm[t,i])
TP_cbraw[t,i]<-exp(TP_cb[t,i])
TPprec_cb[t,i]<-1/log(1+pow(0.15*TP_cbraw[t,i],2)/pow(TP_cbraw[t,i],2))
TP_cb[t,i]~dnorm(TPobsint_cb[t,i],TPprec_cb[t,i])
TPobsint_cb[t,i]~dnorm(TPmodel_cb[t,i],tau)
outflow_cb[t,i]<-volume_cb[t,i]/ResidenceTime_cbm[t]
phi_cb_1[t,i]<-(1/zint_cb[t,i])-pow((1/zint_cb[t,i]),3)/3+pow((1/zint_cb[t,i]),5)/5-pow((1/zint_cb[t,i]),7)/7
phi_cb_2[t,i]<-zint_cb[t,i]-pow(zint_cb[t,i],3)/3+pow(zint_cb[t,i],5)/5-pow(zint_cb[t,i],7)/7
```

```
phi_cb[t,i]<-step(zint_cb[t,i]-1)*((-1)* phi_cb_1[t,i]+1.570796)+step(1-zint_cb[t,i])*phi_cb_2[t,i]
zint_cb[t,i]<-omega/lamda_cb[t,i]
lamda_cb[t,i]<-outflow_cb[t,i]/volume_cb[t,i]+v_cb[t]
                    }
v_cb[t]<-sedimentation_cb[t]/365
Wmean_cb[t]<-(1000000)*Wmean_cbm[t]
Wamp_cb[t]<-(1000000)*Wamp_cbm[t]
                    }
for (t in 1:L){
Wmean_cbm[t]~dnorm(Wmean_cbreg[t],Wmean_cbreg_tau[t])I(Wmean_cbreg_min[t],)
Wmean_cbreg_min[t]<-0.9*Wmean_cbreg[t]
Wmean_cbreg_tau[t]<-1/pow(Wmean_cbRMSE_sb[t]/3,2)
Wamp_cbm[t]<-Wamp_cbreg[t]
theta_cb[t]<-theta_cbreg[t]
}
for (t in 1:L){
    for (i in 1:M) {
TPmodel_kbm[t,i]<-max(0.0001,Wmean_kb[t]/(lamda_kb[t,i]*volume_kb[t,i])
                    +(Wamp_kb[t]/(volume_kb[t,i]*sqrt(pow(lamda_kb[t,i],2)
                    +pow(omega_kb[t],2))))*sin(omega_kb[t]*time[t,i]-theta_kb[t]-phi_kb[t,i]))

TPmodel_kb[t,i]<-log(TPmodel_kbm[t,i])
TP_kbraw[t,i]<-exp(TP_kb[t,i])
TPprec_kb[t,i]<-1/log(1+pow(0.15*TP_kbraw[t,i],2)/pow(TP_kbraw[t,i],2))
TP_kb[t,i]~dnorm(TPobsint_kb[t,i],TPprec_kb[t,i])
TPobsint_kb[t,i]~dnorm(TPmodel_kb[t,i],tau)
outflow_kb[t,i]<-volume_kb[t,i]/ResidenceTime_kbm[t]
phi_kb_1[t,i]<-(1/zint_kb[t,i])-pow((1/zint_kb[t,i]),3)/3+pow((1/zint_kb[t,i]),5)/5-pow((1/zint_kb[t,i]),7)/7
phi_kb_2[t,i]<-zint_kb[t,i]-pow(zint_kb[t,i],3)/3+pow(zint_kb[t,i],5)/5-pow(zint_kb[t,i],7)/7
phi_kb[t,i]<-step(zint_kb[t,i]-1)*((-1)* phi_kb_1[t,i]+1.570796)+step(1-zint_kb[t,i])*phi_kb_2[t,i]
zint_kb[t,i]<-omega_kb[t]/lamda_kb[t,i]
lamda_kb[t,i]<-outflow_kb[t,i]/volume_kb[t,i]+v_kb[t]
}
v_kb[t]<-sedimentation_kb[t]/365
Wmean_kb[t]<-(1000000)*Wmean_kbm[t]
Wamp_kb[t]<-(1000000)*Wamp_kbm[t]
}

for (t in 1:L){
Wmean_kbm[t]~dnorm(Wmean_kbreg[t],Wmean_kbreg_tau[t])I(Wmean_kbreg_min[t],)
Wmean_kbreg_min[t]<-0.9*Wmean_kbreg[t]
Wmean_kbreg_tau[t]<-1/pow(Wmean_kbRMSE_sb[t]/3,2)
Wamp_kbm[t]<-Wamp_kbreg[t]
theta_kb[t]<-theta_kbreg[t]
}
omega_kb[1]<-omega
omega_kb[2]<-omega
omega_kb[3]<-2*omega
omega_kb[4]<-omega
omega_kb[5]<-omega
```

```
for (t in 1:L){
    for (i in 1:M) {
TPmodel_ebm[t,i]<-max(0.0001,Wmean_eb[t]/(lamda_eb[t,i]*volume_ebcor[t,i])
                    +(Wamp_eb[t]/(volume_ebcor[t,i]*sqrt(pow(lamda_eb[t,i],2)
                    +pow(omega,2))))*sin(omega*time[t,i]-theta_eb[t]-phi_eb[t,i]))

TPmodel_eb[t,i]<-log(TPmodel_ebm[t,i])
TP_ebraw[t,i]<-exp(TP_eb[t,i])
TPprec_eb[t,i]<-1/log(1+pow(0.15*TP_ebraw[t,i],2)/pow(TP_ebraw[t,i],2))
TP_eb[t,i]~dnorm(TPobsint_eb[t,i],TPprec_eb[t,i])
TPobsint_eb[t,i]~dnorm(TPmodel_eb[t,i],tau)
outflow_eb[t,i]<-volume_ebcor[t,i]/ResidenceTime_ebm[t]
phi_eb_1[t,i]<-(1/zint_eb[t,i])-pow((1/zint_eb[t,i]),3)/3+pow((1/zint_eb[t,i]),5)/5-pow((1/zint_eb[t,i]),7)/7
phi_eb_2[t,i]<-zint_eb[t,i]-pow(zint_eb[t,i],3)/3+pow(zint_eb[t,i],5)/5-pow(zint_eb[t,i],7)/7
phi_eb[t,i]<-step(zint_eb[t,i]-1)*((-1)* phi_eb_1[t,i]+1.570796)+step(1-zint_eb[t,i])*phi_eb_2[t,i]
zint_eb[t,i]<-omega/lamda_eb[t,i]
volume_ebcor[t,i]<-volume_eb[t,i]*10
lamda_eb[t,i]<-outflow_eb[t,i]/volume_ebcor[t,i]+v_eb[t]
}
v_eb[t]<-sedimentation_eb[t]/365
Wmean_eb[t]<-(1000000)*Wmean_ebm[t]
Wamp_eb[t]<-(1000000)*Wamp_ebm[t]
}
for (t in 1:L){
Wmean_ebm[t]~dnorm(Wmean_ebreg[t],Wmean_ebreg_tau[t])I(Wmean_ebreg_min[t],)
Wmean_ebreg_min[t]<-0.9*Wmean_ebreg[t]
Wmean_ebreg_tau[t]<-1/pow(Wmean_ebRMSE_sb[t]/3,2)
Wamp_ebm[t]<-Wamp_ebreg[t]
theta_eb[t]<-theta_ebreg[t]
}

for (t in 1:L){
    for (i in 1:M) {
TPmodel_mbm[t,i]<-max(0.0001,TPmodel_mb1[t,i]+TPmodel_mb2[t,i]+TPmodel_mb3[t,i])

TPmodel_mb1[t,i]<-(outflow_cb[t,i]*Wmean_cb[t])/(lamda_cb[t,i]*lamda_mb[t,i]*volume_cb[t,i]
                    *volume_mbcor[t,i])
                    +(outflow_kb[t,i]*Wmean_kb[t])/(lamda_kb[t,i]*lamda_mb[t,i]*volume_kb[t,i]
                    *volume_mbcor[t,i])
                    +(outflow_eb[t,i]*Wmean_eb[t])/(lamda_eb[t,i]*lamda_mb[t,i]*volume_ebcor[t,i]
                    *volume_mbcor[t,i])
                    +Wmean_mb[t]/(lamda_mb[t,i]*volume_mbcor[t,i])
TPmodel_mb2[t,i]<-(Wamp_mb[t]/(volume_mbcor[t,i]*sqrt(pow(lamda_mb[t,i],2)
                    +pow(omega,2))))*sin(omega*time[t,i]-theta_mb[t]-phi_mb[t,i])
                    +((outflow_cb[t,i]*Wamp_cb[t])/(volume_cb[t,i]*volume_mbcor[t,i]
                    *sqrt(pow(lamda_cb[t,i],2)
                    +pow(omega,2))*sqrt(pow(lamda_mb[t,i],2)+pow(omega,2))))
                    *sin(omega*time[t,i]-theta_cb[t]-phi_cb[t,i]-phi_mb[t,i])
TPmodel_mb3[t,i]<-((outflow_kb[t,i]*Wamp_kb[t])/(volume_kb[t,i]*volume_mbcor[t,i]
                    *sqrt(pow(lamda_kb[t,i],2)
                    +pow(omega_kb[t],2))*sqrt(pow(lamda_mb[t,i],2)+pow(omega,2))))
```

```
                    *sin(omega_kb[t]*time[t,i]-theta_kb[t]-phi_kb[t,i]-phi_mb[t,i])
                    +((outflow_eb[t,i]*Wamp_eb[t])/(volume_ebcor[t,i]*volume_mbcor[t,i]
                    *sqrt(pow(lamda_eb[t,i],2)+pow(omega,2))*sqrt(pow(lamda_mb[t,i],2)
                    +pow(omega,2))))*sin(omega*time[t,i]-theta_eb[t]-phi_eb[t,i]-phi_mb[t,i])

TPmodel_mb[t,i]<-log(TPmodel_mbm[t,i])
TP_mbraw[t,i]<-exp(TP_mb[t,i])
TPprec_mb[t,i]<-1/log(1+pow(0.15*TP_mbraw[t,i],2)/pow(TP_mbraw[t,i],2))
TP_mb[t,i]~dnorm(TPobsint_mb[t,i],TPprec_mb[t,i])
TPobsint_mb[t,i]~dnorm(TPmodel_mb[t,i],tau)
outflow_mb[t,i]<-volume_mbcor[t,i]/ResidenceTime_mbm[t]
phi_mb_1[t,i]<-(1/zint_mb[t,i])-pow((1/zint_mb[t,i]),3)/3+pow((1/zint_mb[t,i]),5)/5-pow((1/zint_mb[t,i]),7)/7
phi_mb_2[t,i]<-zint_mb[t,i]-pow(zint_mb[t,i],3)/3+pow(zint_mb[t,i],5)/5-pow(zint_mb[t,i],7)/7
phi_mb[t,i]<-step(zint_mb[t,i]-1)*((-1)* phi_mb_1[t,i]+1.570796)+step(1-zint_mb[t,i])*phi_mb_2[t,i]
zint_mb[t,i]<-omega/lamda_mb[t,i]
volume_mbcor[t,i]<-volume_mb[t,i]*10
lamda_mb[t,i]<-outflow_mb[t,i]/volume_mbcor[t,i]+v_mb[t]
}
v_mb[t]<-sedimentation_mb[t]/365
outflow_mbavg[t]<-mean(outflow_mb[t,])
Wmean_mb[t]<-(1000000)*Wmean_mbm[t]
Wamp_mb[t]<-(1000000)*Wamp_mbm[t]
}
for (t in 1:L){
Wmean_mbm[t]~dnorm(Wmean_mbreg[t],Wmean_mbreg_tau[t])I(Wmean_mbreg_min[t],)
Wmean_mbreg_min[t]<-0.9*Wmean_mbreg[t]
Wmean_mbreg_tau[t]<-1/pow(Wmean_mbRMSE_sb[t]/3,2)
Wamp_mbm[t]<-Wamp_mbreg[t]
theta_mb[t]<-theta_mbreg[t]
}

for (t in 1:L){
    for (i in 1:M) {
TPmodel_anm[t,i]<-max(0.0001,TPmodel_an1[t,i]+TPmodel_an2[t,i]+TPmodel_an3[t,i]
                    +TPmodel_an4[t,i]+TPmodel_an5[t,i]+TPmodel_an6[t,i]+TPmodel_an7[t,i]
                    +TPmodel_an8[t,i])

TPmodel_an1[t,i]<-(outflow_mb[t,i]*outflow_cb[t,i]*Wmean_cb[t])/(lamda_an[t,i]*volume_an[t,i]
                    * lamda_cb[t,i]*lamda_mb[t,i]*volume_cb[t,i]*volume_mbcor[t,i])
                    +(outflow_mb[t,i]*outflow_kb[t,i]*Wmean_kb[t])/(lamda_an[t,i]*volume_an[t,i]
                    *lamda_kb[t,i]*lamda_mb[t,i]*volume_kb[t,i]*volume_mbcor[t,i])
                    +(outflow_mb[t,i]*outflow_eb[t,i]*Wmean_eb[t])/(lamda_an[t,i]*volume_an[t,i]
                    *lamda_eb[t,i]*lamda_mb[t,i]*volume_ebcor[t,i]*volume_mbcor[t,i])
TPmodel_an2[t,i]<-(outflow_mb[t,i]*Wmean_mb[t])/(lamda_an[t,i]*volume_an[t,i]*lamda_mb[t,i]
                    *volume_mbcor[t,i])
TPmodel_an3[t,i]<-Wmean_an[t]/(lamda_an[t,i]*volume_an[t,i])
TPmodel_an4[t,i]<-(Wamp_an[t]/(volume_an[t,i]*sqrt(pow(lamda_an[t,i],2)+pow(omega,2))))
                    *sin(omega*time[t,i]-theta_an[t]-phi_an[t,i])
TPmodel_an5[t,i]<-((outflow_mb[t,i]*Wamp_mb[t])/(volume_mbcor[t,i]*volume_an[t,i]
                    *sqrt(pow(lamda_mb[t,i],2)+pow(omega,2))*sqrt(pow(lamda_an[t,i],2)
                    +pow(omega,2))))*sin(omega*time[t,i]-theta_mb[t]-phi_mb[t,i]-phi_an[t,i])
```

```
TPmodel_an6[t,i]<-((outflow_mb[t,i]*outflow_cb[t,i]*Wamp_cb[t])/(volume_an[t,i]*volume_cb[t,i]
                  *volume_mbcor[t,i]*sqrt(pow(lamda_cb[t,i],2)+pow(omega,2))*sqrt(pow(lamda_mb[t,i],2)
                  +pow(omega,2))*sqrt(pow(lamda_an[t,i],2)+pow(omega,2))))*sin(omega*time[t,i]
                  -theta_cb[t]-phi_cb[t,i]-phi_mb[t,i]-phi_an[t,i])
TPmodel_an7[t,i]<-((outflow_mb[t,i]*outflow_kb[t,i]*Wamp_kb[t])/(volume_an[t,i]*volume_kb[t,i]
                   *volume_mbcor[t,i]*sqrt(pow(lamda_kb[t,i],2)+pow(omega_kb[t],2))
                   *sqrt(pow(lamda_mb[t,i],2)+pow(omega,2))*sqrt(pow(lamda_an[t,i],2)
                   +pow(omega,2))))*sin(omega_kb[t]*time[t,i]-theta_kb[t]-phi_kb[t,i]
                   -phi_mb[t,i]-phi_an[t,i])

TPmodel_an8[t,i]<-((outflow_mb[t,i]*outflow_eb[t,i]*Wamp_eb[t])/(volume_an[t,i]*volume_ebcor[t,i]
                  *volume_mbcor[t,i]*sqrt(pow(lamda_eb[t,i],2)+pow(omega,2))*sqrt(pow(lamda_mb[t,i],2)
                  +pow(omega,2))*sqrt(pow(lamda_an[t,i],2)+pow(omega,2))))*sin(omega*time[t,i]
                  -theta_eb[t]-phi_eb[t,i]-phi_mb[t,i]-phi_an[t,i])

TPmodel_an[t,i]<-log(TPmodel_anm[t,i])
TP_anraw[t,i]<-exp(TP_an[t,i])
TPprec_an[t,i]<-1/log(1+pow(0.15*TP_anraw[t,i],2)/pow(TP_anraw[t,i],2))
TP_an[t,i]~dnorm(TPobsint_an[t,i],TPprec_an[t,i])
TPobsint_an[t,i]~dnorm(TPmodel_an[t,i],tau)
outflow_an[t,i]<-volume_an[t,i]/ResidenceTime_anm[t]
phi_an_1[t,i]<-(1/zint_an[t,i])-pow((1/zint_an[t,i]),3)/3+pow((1/zint_an[t,i]),5)/5-pow((1/zint_an[t,i]),7)/7
phi_an_2[t,i]<-zint_an[t,i]-pow(zint_an[t,i],3)/3+pow(zint_an[t,i],5)/5-pow(zint_an[t,i],7)/7
lamda_an[t,i]<-outflow_an[t,i]/volume_an[t,i]+v_an[t]
phi_an[t,i]<-step(zint_an[t,i]-1)*((-1)* phi_an_1[t,i]+1.570796)+step(1-zint_an[t,i])*phi_an_2[t,i]
zint_an[t,i]<-omega/lamda_an[t,i]

}
v_an[t]<-sedimentation_an[t]/365
TPRetention[t]<-
TPmodel_anmavg[t]*outflow_anavg[t]/(Wmean_an[t]+Wmean_mb[t]+Wmean_eb[t]+Wmean_kb[t]+Wmean
_cb[t])
TWoutput[t]<-(TPmodel_anmavg[t]*outflow_anavg[t]/1000000)*365/1000
TWmean[t]<-
((Wmean_an[t]+Wmean_mb[t]+Wmean_eb[t]+Wmean_kb[t]+Wmean_cb[t])/1000000)*365/1000
TPmodel_anmavg[t]<-mean(TPmodel_anm[t,])
outflow_anavg[t]<-mean(outflow_an[t,])
Wmean_an[t]<-(1000000)*Wmean_anm[t]
Wamp_an[t]<-(1000000)*Wamp_anm[t]
}

for (t in 1:L){
Wmean_anm[t]~dnorm(Wmean_anreg[t],Wmean_anreg_tau[t])I(Wmean_anreg_min[t],)
Wmean_anreg_min[t]<-0.9*Wmean_anreg[t]
Wmean_anreg_tau[t]<-1/pow(Wmean_anRMSE_sb[t]/3,2)
Wamp_anm[t]<-Wamp_anreg[t]
theta_an[t]<-theta_anreg[t]
}

for (t in 1:L){
      sedimentation_cb[t]~dnorm(gv,gtau[1])I(0,)
```

```
        sedimentation_kb[t]~dnorm(gv,gtau[2])I(0,)
        sedimentation_eb[t]~dnorm(gv,gtau[3])I(0,)
        sedimentation_mb[t]~dnorm(gv,gtau[4])I(0,)
        sedimentation_an[t]~dnorm(gv,gtau[5])I(0,)
        ResidenceTime_cbm[t]~dnorm(ResidenceTime_cb,ResidenceTime_cb.tau)I(0,)
        ResidenceTime_kbm[t]~dnorm(ResidenceTime_kb,ResidenceTime_kb.tau)I(0,)
        ResidenceTime_ebm[t]~dnorm(ResidenceTime_eb,ResidenceTime_eb.tau)I(0,)
        ResidenceTime_mbm[t]~dnorm(ResidenceTime_mb,ResidenceTime_mb.tau)I(0,)
        ResidenceTime_anm[t]~dnorm(ResidenceTime_an,ResidenceTime_an.tau)I(0,)
            }
for (i in 1:5){
gtau[i]~dgamma(0.001,0.001)
gsigma[i]<-sqrt(1/gtau[i])}

gv~dnorm(gvmu,gvtau)
gvmu~dnorm(0,0.0001)I(0,)
gvtau~dgamma(0.001,0.001)
gvsigma<-sqrt(1/gvtau)

ResidenceTime_cb.tau<-1/pow(0.25*ResidenceTime_cb,2)
ResidenceTime_kb.tau<-1/pow(0.25*ResidenceTime_kb,2)
ResidenceTime_eb.tau<-1/pow(0.25*ResidenceTime_eb,2)
ResidenceTime_mb.tau<-1/pow(0.25*ResidenceTime_mb,2)
ResidenceTime_an.tau<-1/pow(0.05*ResidenceTime_an,2)

omega<-2*3.1415/365
tau~dgamma(0.001,0.001)
sigma<-sqrt(1/tau)
}
```

Inference Data

list(L=5, M=7,time=structure(.Data=c(***paste time5.dat here***),.Dim=c(5,7)),
TP_cb=structure(.Data=c(***paste TPcb.dat here***),.Dim=c(5,7)),
volume_cb=structure(.Data=c(***paste Volumecb.dat here***),.Dim=c(5,7)),
TP_kb=structure(.Data=c(***paste TPkb.dat here***),.Dim=c(5,7)),
volume_kb=structure(.Data=c(***paste Volumekb.dat here***),.Dim=c(5,7)),
TP_eb=structure(.Data=c(***paste TPeb.dat here***),.Dim=c(5,7)),
volume_eb=structure(.Data=c(***paste Volumeeb.dat here***),.Dim=c(5,7)),
TP_mb=structure(.Data=c(***paste TPmb.dat here***),.Dim=c(5,7)),
volume_mb=structure(.Data=c(***paste Volumemb.dat here***),.Dim=c(5,7)),
TP_an=structure(.Data=c(***paste TPan.dat here***),.Dim=c(5,7)),
volume_an=structure(.Data=c(***paste Volumean.dat here***),.Dim=c(5,7)),

ResidenceTime_cb=429,
ResidenceTime_kb=477,
ResidenceTime_eb=2887,
ResidenceTime_mb=3265,
ResidenceTime_an=79,

Wmean_kbreg=c(***paste Wmean_kb.dat here***),
Wmean_kbRMSE_sb=c(***paste Wmean_kbRMSE.dat here***),

Wamp_kbreg=c(***paste Wamp_kb.dat here***),
theta_kbreg=c(***paste theta_kb.dat here***),

Wmean_cbreg=c(***paste Wmean_cb.dat here***),
Wmean_cbRMSE_sb=c(***paste Wmean_cbRMSE.dat here***),
Wamp_cbreg=c(***paste Wamp_cb.dat here***),
theta_cbreg=c(***paste theta_cb.dat here***),

Wmean_mbreg=c(***paste Wmean_mb.dat here***),
Wmean_mbRMSE_sb=c(***paste Wmean_mbRMSE.dat here***),
Wamp_mbreg=c(***paste Wamp_mb.dat here***),
theta_mbreg=c(***paste theta_mb.dat here***),

Wmean_ebreg=c(***paste Wmean_eb.dat here***),
Wmean_ebRMSE_sb=c(***paste Wmean_ebRMSE.dat here***),
Wamp_ebreg=c(***paste Wamp_eb.dat here***),
theta_ebreg=c(***paste theta_eb.dat here***),

Wmean_anreg=c(***paste Wmean_an.dat here***),
Wmean_anRMSE_sb=c(***paste Wmean_anRMSE.dat here***),
Wamp_anreg=c(***paste Wamp_an.dat here***),
theta_anreg=c(***paste theta_an.dat here***))

Initial values 1

list(
sedimentation_cb=c(0.005,0.005,0.005,0.005,0.005),
sedimentation_kb=c(0.005,0.005,0.005,0.005,0.005),
sedimentation_eb=c(0.005,0.005,0.005,0.005,0.005),
sedimentation_mb=c(0.005,0.005,0.005,0.005,0.005),
sedimentation_an=c(0.005,0.005,0.005,0.005,0.005),
gv=0.005,
gvmu=0.005,
gtau=c(0.1,0.1,0.1,0.1,0.1),
gvtau=0.1,
ResidenceTime_cbm=c(429,429,429,429,429),
ResidenceTime_kbm=c(477,477,477,477,477),
ResidenceTime_ebm=c(2887,2887,2887,2887,2887),
ResidenceTime_mbm=c(3265,3265,3265,3265,3265),
ResidenceTime_anm=c(79,79,79,79,79),
tau=0.1,
Wmean_kbm=c(***paste Wmean_kbm.dat here***),
Wmean_cbm=c(***paste Wmean_cbm.dat here***),
Wmean_mbm=c(***paste Wmean_mbm.dat here***),
Wmean_ebm=c(***paste Wmean_ebm.dat here***),
Wmean_anm=c(***paste Wmean_anm.dat here***),
TPobsint_cb=structure(.Data=c(***paste TPobs_cb.dat here***),.Dim=c(5,7)),
TPobsint_kb=structure(.Data=c(***paste TPobs_kb.dat here***),.Dim=c(5,7)),
TPobsint_eb=structure(.Data=c(***paste TPobs_eb.dat here***),.Dim=c(5,7)),
TPobsint_mb=structure(.Data=c(***paste TPobs_mb.dat here***),.Dim=c(5,7)),
TPobsint_an=structure(.Data=c(***paste TPobs_an.dat here***),.Dim=c(5,7)))

Initial values 2

list(
sedimentation_cb=c(0.0075,0.0075,0.0075,0.0075,0.0075),
sedimentation_kb=c(0.0075,0.0075,0.0075,0.0075,0.0075),
sedimentation_eb=c(0.0075,0.0075,0.0075,0.0075,0.0075),
sedimentation_mb=c(0.0075,0.0075,0.0075,0.0075,0.0075),
sedimentation_an=c(0.0075,0.0075,0.0075,0.0075,0.0075),
gv=0.0075,
gvmu=0.0075,
gtau=c(0.25,0.25,0.25,0.25,0.25),
gvtau=0.25,
ResidenceTime_cbm=c(435,435,435,435,435),
ResidenceTime_kbm=c(485,485,485,485,485),
ResidenceTime_ebm=c(2897,2897,2897,2897,2897),
ResidenceTime_mbm=c(3275,3275,3275,3275,3275),
ResidenceTime_anm=c(89,89,89,89,89),
tau=0.25,
Wmean_kbm=c(***paste Wmean_kbm.dat here***),
Wmean_cbm=c(***paste Wmean_cbm.dat here***),
Wmean_mbm=c(***paste Wmean_mbm.dat here***),
Wmean_ebm=c(***paste Wmean_ebm.dat here***),
Wmean_anm=c(***paste Wmean_anm.dat here***),
TPobsint_cb=structure(.Data=c(***paste TPobs_cb.dat here***),.Dim=c(5,7)),
TPobsint_kb=structure(.Data=c(***paste TPobs_kb.dat here***),.Dim=c(5,7)),
TPobsint_eb=structure(.Data=c(***paste TPobs_eb.dat here***),.Dim=c(5,7)),
TPobsint_mb=structure(.Data=c(***paste TPobs_mb.dat here***),.Dim=c(5,7)),
TPobsint_an=structure(.Data=c(***paste TPobs_an.dat here***),.Dim=c(5,7)))